Proceedings World Geothermal Congress 2015
Melbourne, Australia, 19-25 April 2015

Development of an Engineered Geothermal System Exploration Methodology Using the Dixie Valley Geothermal Area, Nevada USA, as a Laboratory Calibration Site System

Joe Iovenitti[1], Ileana M. Tibuleac[2], Philip Wannamaker[3], Robert Karlin[4], Fletcher H. Ibser[5], David Blackwell[6] and Jon Sainsbury[7]

11470 Creekside Drive, Unit No. 23, Walnut Creek, California 94596, USA
2University of Nevada Reno, Nevada Seismological Laboratory, Reno, Nevada 89557, USA
3Univeristy of Utah, Energy and Geoscience Institute, Salt Lake City, Utah 84108, USA
4University of Nevada Reno, Department of Geology, Reno, Nevada 89557, USA
5University of California, Berkeley, Department of Statistics, Berkeley, California 94720, USA
6Southern Methodist University, Department of Earth Sciences, Dallas, Texas 75275, USA
71382 Aralia Court, San Luis Obispo, California 93401, USA

joeiovenitti@comcast.net

Keywords: EGS, Hydrothermal System, Exploration Methods, Geostatistics, Favorability/Trust Mapping

ABSTRACT

The Dixie Valley Geothermal Area, a Basin and Range type system, in central Nevada USA was chosen as the calibration site for development of an Engineered Geothermal system exploration methodology development due to its extensive body of geoscience data and information on the geothermal system and most importantly, well results in the public domain. It is also has the highest reported bottomhole temperature, 285°C, in the Basin and Range and the geothermal field is generating over 60 MWs of electrical power. The overall project study area was 2500km^2 with a calibration area (defined by the existing wellfield) of approximately 170km^2. A baseline (existing data) analysis was conducted, and on this basis, baseline favorability maps were generated, from +1km above sea level (asl) to -4km asl at 0.5km intervals, for the three key Engineered Geothermal System (EGS) parameters of interest: rock type, temperature, and stress. Complimentary baseline trust ("confidence-in-the-data-used") maps were also created at the same scale to, among other things, indicate where additional data was required. Exploratory geostatistical data analysis was also conducted to determine the predictability of several key attributes of the system. To reduce data uncertainty and geophysical data and information non-uniqueness, new gravity, magnetotelluric, and ambient seismic noise data were collected to supplement the baseline data set. The enhanced data set (baseline + new data) were modeled and interpreted along with enhanced thermal modeling and enhanced geostatistical analysis. The outcome of both the baseline and enhanced data analysis are presented.

1. INTRODUCTION

MIT (2006) estimated the total Enhanced Geothermal System (EGS) resource base in the United States (US) to be greater than 13 million exajoules (3.6x10^{15} MWh). The USGS (2008) estimated the mean electric power resource for EGS on private and accessible public land in the US as 517,800 MWe, with a 95% probability of 345,100 MWe and a 5% probability of 727,900 MWe. Not to make an understatement, the resource base is large. However, to date, there is no widely accepted, invasive or non-invasive exploratory methodology for “greenfield” EGS sites proven to be both technically feasible and cost effective. Drilling slimholes to identify the actual resource base allows direct identification and measurement of the primary EGS resource critical geoscience parameters, temperature (T), lithology and stress regime, but widespread use of this methodology is cost prohibitive and as such, must be used selectively. Developing a cost effective and reliable exploration methodology is essential for the economic viability of EGS in regions beyond what has already been explored for hydrothermal resources.

This paper describes the results of a systematic investigation, of some primary exploration methods and results used in the Dixie Valley Geothermal System (DVGS), a Basin and Range (B&R) system, in central Nevada, USA, to attempt calibration of these methods using data and information from the Dixie Valley Geothermal Wellfield (DVGW, also referred to herein as the calibration area). Figure 1 presents both the project area and calibration areas investigated. The project area size, 50 kilometer (km) x 50km, was center over the DVGW and defined by the requirement for high-resolution geophysical data. The DVGW was chosen as the field calibration site for this investigation because, in the public domain, it is a highly characterized B&R geothermal system with a considerable amount of geoscience data and information including exploratory, production, injection and dry well data. The wellfield has approximately 30 wells, for which the project had lithologic data from 22 of them and bottomhole (BHT) data for 26 wells, T-depth profiles for 10 wells. The DVGS is also the hottest known B&R geothermal system with a measured BHT of 285°C in well 36-14, a sub-producer. The DVGW is generating 62 MWs of electric power from a dual-flash plant since 1988 (Benoit, 2013).

To assess the EGS conditions of the project area, an overall geoscience evaluation of the project area was conducted with a focus on the DVGW for exploration methodology calibration purposes. Statistical relationships between select

geoscience parameters were performed to quantify parameter relationships and determine the predictive powers of various parameters.

The study was divided into two parts. The first part involved (1) assessing the existing (baseline) data and information, (2) developing a baseline conceptual model for the DVGW, (3) performing baseline geostatistical exploratory data analysis on select geoscience parameters, and (4) generating complimentary favorability and trust maps based on the three primary EGS resource characteristics (see above). A trust map presents the "confidence in the data used" in preparing the favorability depth slice map. The second part consisted of (1) collecting new geophysical and geochemical data to reduce some of the uncertainty and non-uniqueness in the baseline conceptual model, (2) developing an enhanced (baseline plus new data and information) conceptual model, and (3) conducting enhanced data geostatistical analysis. The overarching goals of this project was to calibrate the exploration methods used and identify potential EGS drilling targets.

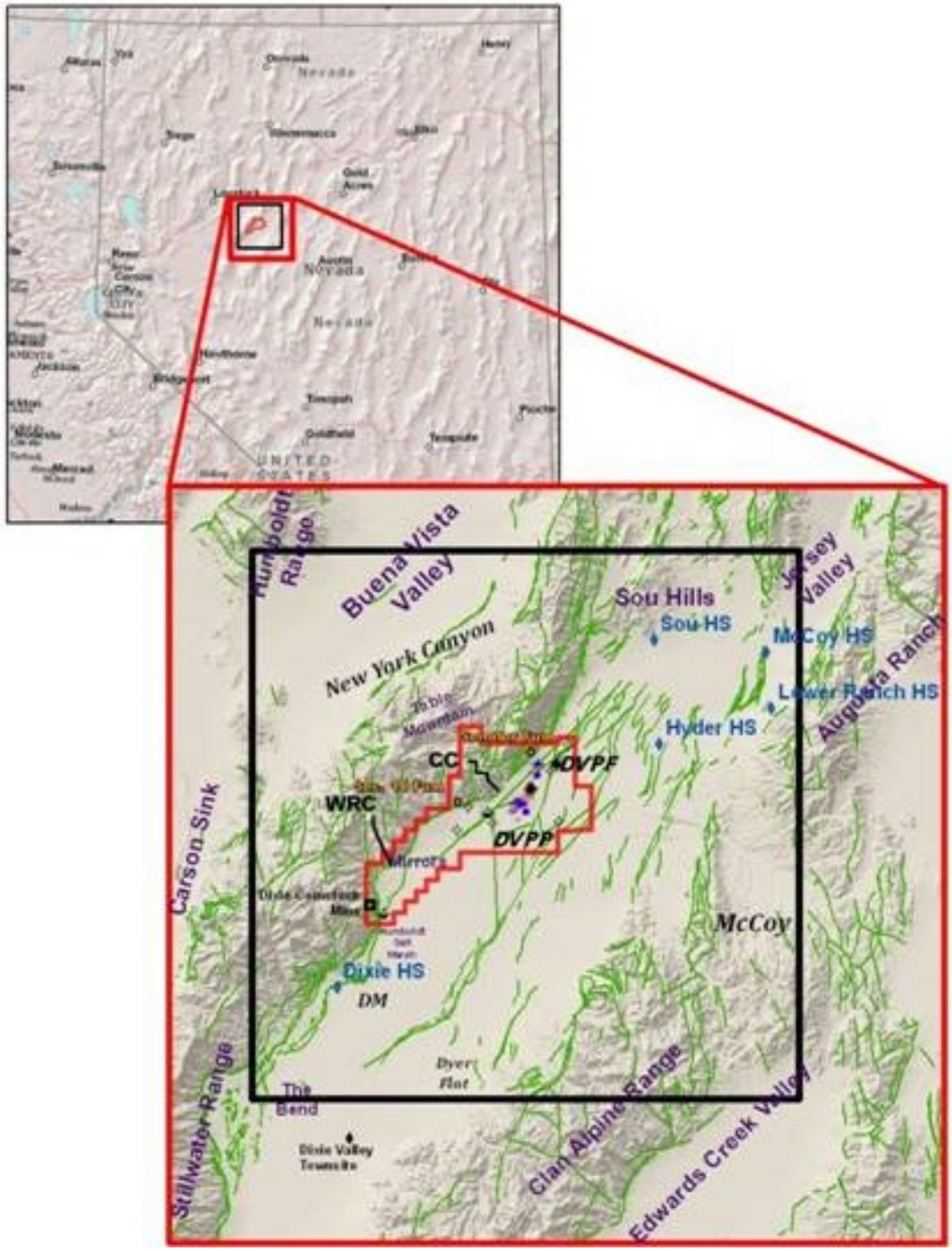

Figure 1: EGS Exploration Methodology project area (black square) is 50km by 50km. The Dixie Valley Geothermal Wellfield (DVGW, the project calibration area), outlined in red encompasses approximately 170km^2. Major known and inferred faulting is shown in green. Geographic features are identified along with hot springs and two properties within the DVGW (DVPF, the Dixie Valley Producing Field and DVPP, Dixie Valley Power Partners). The figure is after Blackwell et al. (2005).

The results of some of this work has been published at the Geothermal Resources Council annual meetings (Iovenitti et al., 2010, 2011; Thakur et al., 2012) and the Workshop on Geothermal Reservoir Engineering at Stanford University (Iovenitti et al., 2012, 2013; Tibuleac et al. 2013; Wannamaker et al. 2013). The reports on part one of this study (AltaRock, 2014a) and part two (AltaRock, 2014b) are available through the US National Geothermal Data System (http://geothermaldata.org/). This paper presents the salient features of the previously published results for context and presents new information on the enhanced investigation. No attempt is made herein to describe the details of the geoscience setting of the project area. The reader is referred to AltaRock (2014a) for these details.

2. BASELINE INVESTIGATION

The Baseline Investigation component of this investigation consisted of a reviewing the geology (stratigraphy, structure and stress), geophysics (gravity, aeromagnetics, magnetotelluric [MT], seismic and thermal), hydrology, geochemistry; development of a baseline conceptual model integrating all the available data sets, conducting a geostatistical exploratory data analysis, and generating favorability/trust maps. This initial review was facilitated by a comprehensive draft report on the DVGS by Blackwell et al. (2005).

2.1 Geologic Setting of the Geothermal Field

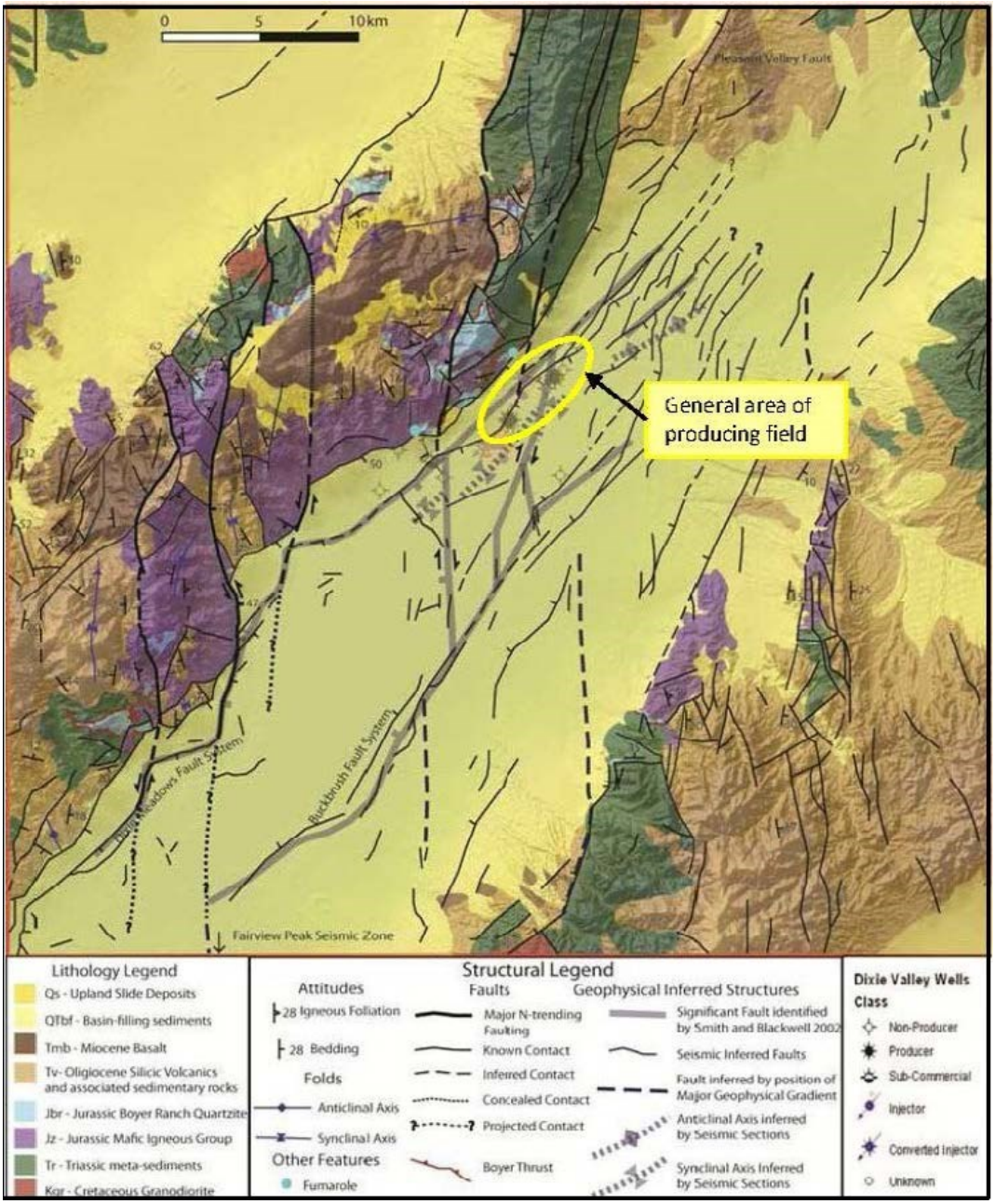

Figure 2: Generalized stratigraphy and structural setting in the project area (red outline) along with some of the wells in the Dixie Valley Geothermal Wellfield. The producing geothermal wellfield lies within the yellow oval. The DVGW is presented in Figures 1. The figure is oriented north-south. Note that for the purposes of this paper the Qs unit has not been considered. The structural setting of the DVGW is complex

The DVGS lies in Dixie Valley and it is bounded to the west by the Stillwater Range. For simplicity, the geologic formations in the project area were divided into seven major and one minor stratigraphic units based on their field occurrence and EGS potential. These units from youngest to oldest are (1) Quaternary-Tertiary basin fill (Q-Tb), Tertiary Miocene basalt (Tmb), Tertiary Oligocene volcanics (Tv), Jurassic Humboldt Igneous Group, (Jz), Jurassic Boyer Ranch Quartzite (Jbr, the minor unit), Triassic meta-sediments (Tr), Cretaceous-Tertiary (?) Granodiorite (Kgr), and Paleozoic meta-sediments (Pz). Figure 2 is a generalized geologic map of the project area with structure based on Smith and Blackwell (2002), among others. The principal stress in the area is NE-SW with extensional B&R normal faulting in the same direction. An older (pre-8 mya) N- to NW-trending B&R structure is also present.

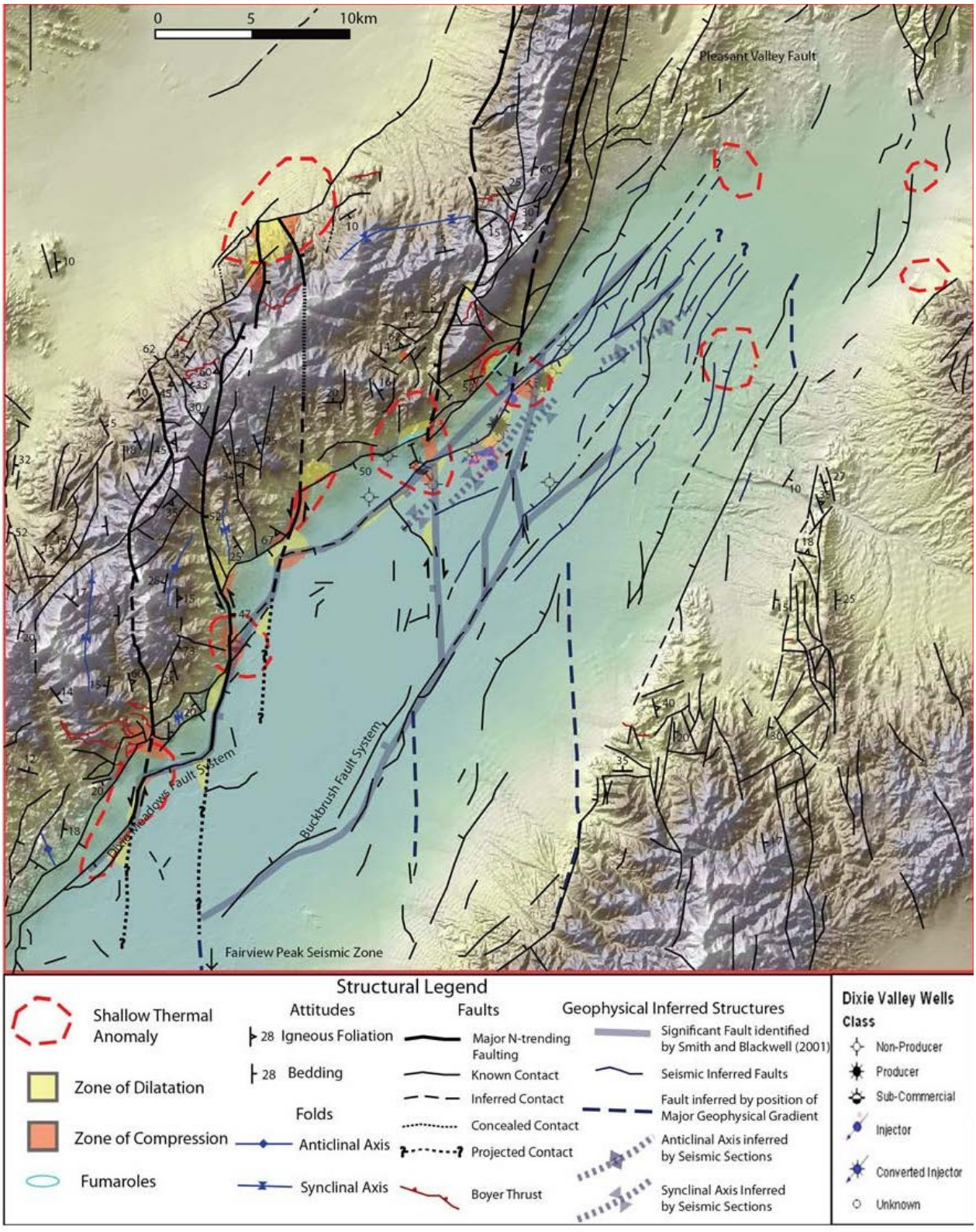

Figure 3: Generalized structural setting of the project are and the occurrence of shallow thermal anomalies and the producing geothermal field.

One of the more unusual features of the Stillwater Range is its highly segmented shape compared to other B&R range fronts which are generally fairly linear. This has been interpreted by the authors to be the result of reactivation of the older N- and NW-trending faults in the current stress field and creating oblique slip along these structures creating regions of dilatation and compression where they intersect the dominant NE-trending range front fault. Figure 3 presents the structural setting of the project are along with shallow thermal anomalies identified by Blackwell et al. (2005). An excellent correlation between the intersection of pre-8 mya N-trending structures (Waibel, 1987) and the NE-trending range front fault with the shallow thermal anomalies on both sides of the Stillwater Range along with the identified dilatation and compression zones whose areal extent were arbitrarily assigned. The dilatation zones are interpreted to host various geothermal cells within an overall Dixie Valley Geothermal District. The structural-thermal anomaly correlation is further supported by the helium R/Ra values (Kennedy and van Soest, 2006) for fumaroles, hot springs, and producing Dixie Valley wells (Figure 4).

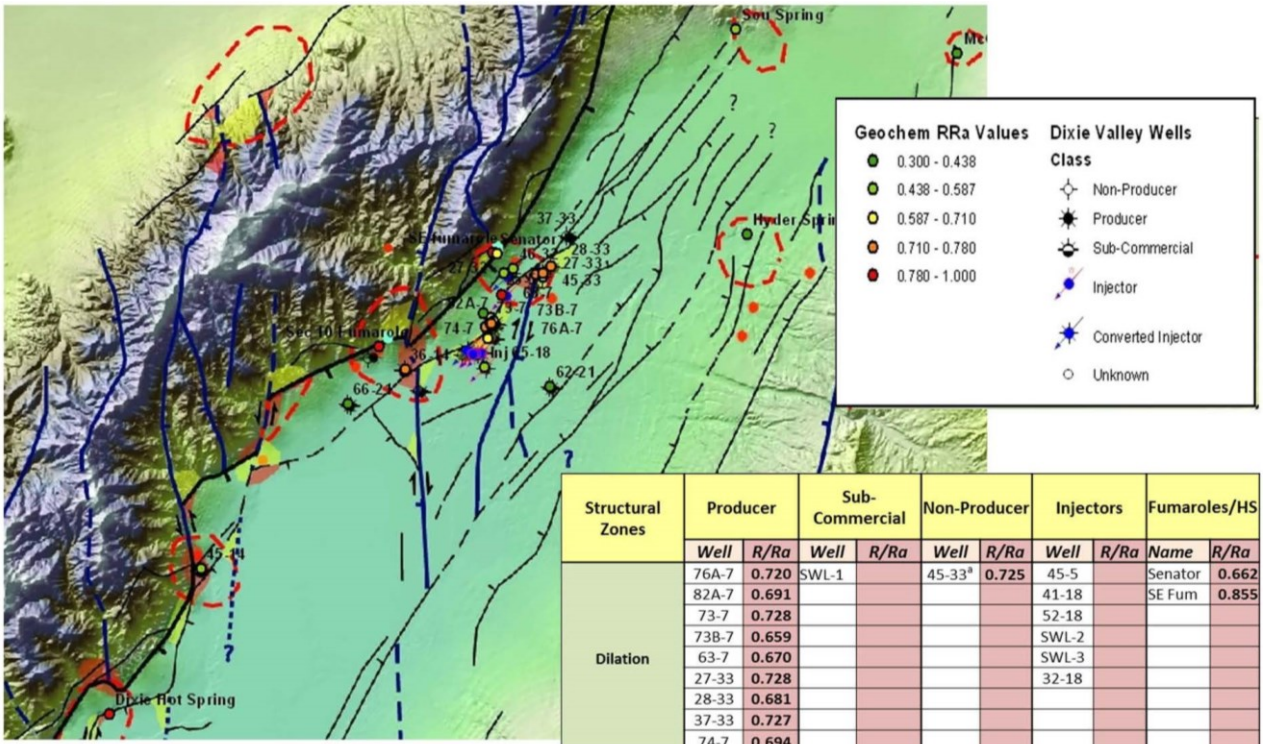

Structural Zones	Producer		Sub-Commercial		Non-Producer		Injectors		Fumaroles/HS	
	Well	*R/Ra*	*Well*	*R/Ra*	*Well*	*R/Ra*	*Well*	*R/Ra*	*Name*	*R/Ra*
Dilation	76A-7	**0.720**	SWL-1		45-33[a]	**0.725**	45-5		Senator	**0.662**
	82A-7	**0.691**					41-18		SE Fum	**0.855**
	73-7	**0.728**					52-18			
	73B-7	**0.659**					SWL-2			
	63-7	**0.670**					SWL-3			
	27-33	**0.728**					32-18			
	28-33	**0.681**								
	37-33	**0.727**								
	74-7	**0.694**								
Compression			36-14	**0.770**	62-23A				Dixie	**0.845**
			45-14	0.587	82-5					
Other			38-32		66-21	0.306	65-18	0.560	Sou	0.528
					62-21		27-32	0.583	Hyder	0.438
					76-28				McCoy	0.345
					53-15				Jersey	0.495

[a]Well data available to AltaRock is limited. It is unknown why this well is a non-producer.

Figure 4: Dixie Valley Geothermal Wellfield well and their helium R/Ra values relative to identified structural zones.

Table 1: Correlation of permeable geologic formations, stress condition and structural zone type

Well Type	Well ID No.	Permeable Interval (m)	Permable Interval Formation[1]	Bottom Hole Formation	Stress Conditions[2] Horizontal Minimum Stress Orientation	Mag.	Stress State	Compression / Dilatation / Other Zone[3]
Injectors	25-5	1800-1900	Tmb	Tmb	Optimal	NA	NA	Dilatation
	37-33	2600-2800	Jz, Jbr	Kgr	Optimal	NA	NA	
	73-7	2650-2700	Jz	Jz	Optimal	low	critically stressed	
	74-7	2600-2700	Jz	Jz	Optimal	low	critically stressed	
Sub-Commerical	**45-14**	NA	NA	Tr	Mis-oriented	low	not critically stressed	Compression
Dry Holes	**66-21**			Tr	Optimal	high	not critically stressed	Other
	82-5			---	Optimal > 2.7km	NA	NA	Compression

[1]Bottom Hole Formations: Tmb-Miocene basalt, Tv-Cz silicic volcanics, Jz-mafic rocks, Tr-metasediments, Kgr-granodiorite
[2]Stress Conditions from Hickman et al. (1998, 2000)
[3]Relative to bottomhole permeable interval; Other Zone indicates the well is completed in neither a zone of compression nor dilatation

Hickman et al. (1998; 2000) conducted a state-of-stress analysis on some of the wells in the DVGW. Table 1 presents the correlation of know stress conditions, geologic formation, and the select well location relative to the structural zone where they occur. Also shown are the permeable intervals and permeable interval formation for select injectors in the DVGW. No other well data was available to this investigation for this stress consideration analysis. These limited data are consistent with the identification of dilatation and compression identified above.

2.2 Baseline Qualitative Geoscience Correlations

A total of eight serial cross-sections traversing the DVGW were constructed using the surface geology, wellfield geology and T, seismic reflection profiles, 2.5D gravity and magnetic modeling, and seismic velocity modeling: six perpendicular to the range-front fault (C-C' to H-H') and two parallel to it. These sections include three MT lines (array lines N, C and S shown in Plate 1) from Wannamaker (2006, 2007) which are directly compared to other geoscience data along sections C-C', E-E' and F-F'). Plate 1 presents the perpendicular serial sections for these datasets with a N45°E view.

The Stillwater Range range-bounding fault on the west side of the geothermal field (Figure 2), has historically been identified as the principal controlling structure for the DVGW (Benoit, 1999) and has been referred to as the Dixie Valley Fault (Caskey et al. 1996) or the Stillwater Fault (Hickman et al., 1998, 2001). The structural setting of the DVGW is complex but current interpretation of the wellfield, gravity-magnetic modeling, have defined a multiple fault system referred to herein as the Dixie Valley Fault Zone (DVFZ). It consists primarily of a steeply-dipping the range-front fault and a piedmont fault(s) with the major offset occurring along the piedmont fault (Plate 1). These structures appear to host two different hydrothermal cells. The range-front fault (section D-D') is interpreted to be the conduit for the highest T in the field (285°C) while production is from the piedmont fault with T on the order of 250°C.

The jointly modeled baseline gravity and magnetics data were consistent with the surface geology and the basement as defined in well 62-21 on the southeastern edge of the DVGW. In an aeromagnetic map superimposed on a geologic map, it was observed that magnetic anomaly highs are closely associated with mafic Jurassic volcanic units exposed in the Stillwater range in almost every instance. For purposes of magnetics modeling, the Jurassic volcanics (Jz= Jg+Jv) were considered the only magnetized units in the area. For gravity modeling, the stratigraphy was subdivided into three other non-magnetic units: fill (Q-Tbf), low density Tertiary rhyolite (Tv) and undifferentiated bedrock (presumably Tr and/or Kgr). Locally a low density unit was required at the top of the valley fill. Additionally, (1) the complex nature and steeply dipping DVFZ is clearly observed in the sections, (2) hydrothermal alteration was thought to be responsible for the discontinuous nature of the magnetized Jz unit and low resistivity identified in the MT sections, and (3) major intra-valley structures bounding the magnetized Jz are approximately coincident with the N-trending structures identified in Figure 2.

While the MT section showed a dominant low-resistivity zone in the valley fill extending to below 10km, superposition of the geology sections indicated a high-level of correlation. The 1000 ohm-meter (Ω-m) region (section E-E' in Plate 1) is attributed to relatively unfractured Kgr. The low resistivity zone in the valley correlated with N-trending structures in arrays S and C (Plate 1 sections C-C' and E-E'). The low resistivity was not attributed active hydrothermal activity but rather to an ancestral alteration zone since T measured in well 62-21 (see section E-E') are comparatively low. MT array C (section E-E') showed ~100 Ω-m around 1-2km range-ward inferring the possibility of intra-range geothermal activity. Low resistivity at the range-front at arrays S and N (sections C-C' and F-F') correlate with surface thermal anomalies.

2.2 Baseline Quantitative Geoscience Correlations

Exploratory geostatistical data analysis was conducted on selected geoscience parameters to investigate the qualitative geoscience correlations, the suggestion by Biasi et al. (2008) that seismic data correlated with T and rock type, and to determine if geostatistical correlations could facilitate EGS favorability map generation. Selected geoscience parameters investigated were rock density, fracture intensity, vertical stress, gravity-magnetic inferred lithology, T, resistivity (derived from MT), seismic parameters: P-and S-wave velocity (Vp and Vs, respectively), and Coulomb Stress Change data (CSC) and dilatation. Additional parameters were considered but not used the analysis as a result of either poor spatial resolution or limited data sets (e.g., well fluid chemistry). The analysis used assigned (inferred), modeled, calculated, or measured data. As such, the data set is not ideal for statistical analysis and the assumption was used that while the exploration data set is statistically not ideal, and some parameters are more reliable than others, the data can be used to determine because whatever uncertainty exists in the different parameters can be thought of as a measurement error, and is at least from a practical standpoint, unbiased. Data parameters were determined for a 500m by 500m grid cell generally from +1km to -4km asl for two datasets: along cross-sections C-F (as illustrated in Plate 1), and with respect to wells and referred to below as sectional and well data, respectively. The latter is considered a much more reliable data set than the former. Geostatistical analyses performed on select geoscience parameters for the individual and combined sections C-F include (1) bivariate (undivided per categorical groups such as lithology); (2) multivariate per stratigraphic formation (e.g., Kgr); and (3) global domain which divides the sectional data into three different geologic environments: Stillwater Range, DVFZ, and the valley; (4) a Classification and Regression Tree (CART) to determine prediction capabilities.

Bivariate, multivariate and domain analyses found T and vertical stress to be independently correlated with Vp and resistivity along the sections C-F, along the sectional data with respect to stratigraphic formation, and along the sectional data with respect to geologic/geographic domains. All other correlations found are not consistent across the three analyses. Discussed below is the Vp-T relationship observed and the CART analysis results.

2.2.2 Empirical Vp-Temperature Relationship

Bivariate (also referred to as global linear correlation analysis in Iovenitti et al. 2012; 2013) of all baseline Vp vs T data had a correlation coefficient of 0.9 (R^2=0.81) while the same analysis for well data indicated a R^2 of 0.51 based on a linear fit that was determined to be skewed by shallow Vp data at the surface (+1km asl). Additionally, outlier data corresponding to certain wells where the modeled Vp trust data was low. Removing the surface data and outlier wells (53-15, 45-14, 66-21 and 76-28) found a polynomial 2-degree fit to the data with a R^2 of 0.72 (Figure 5).

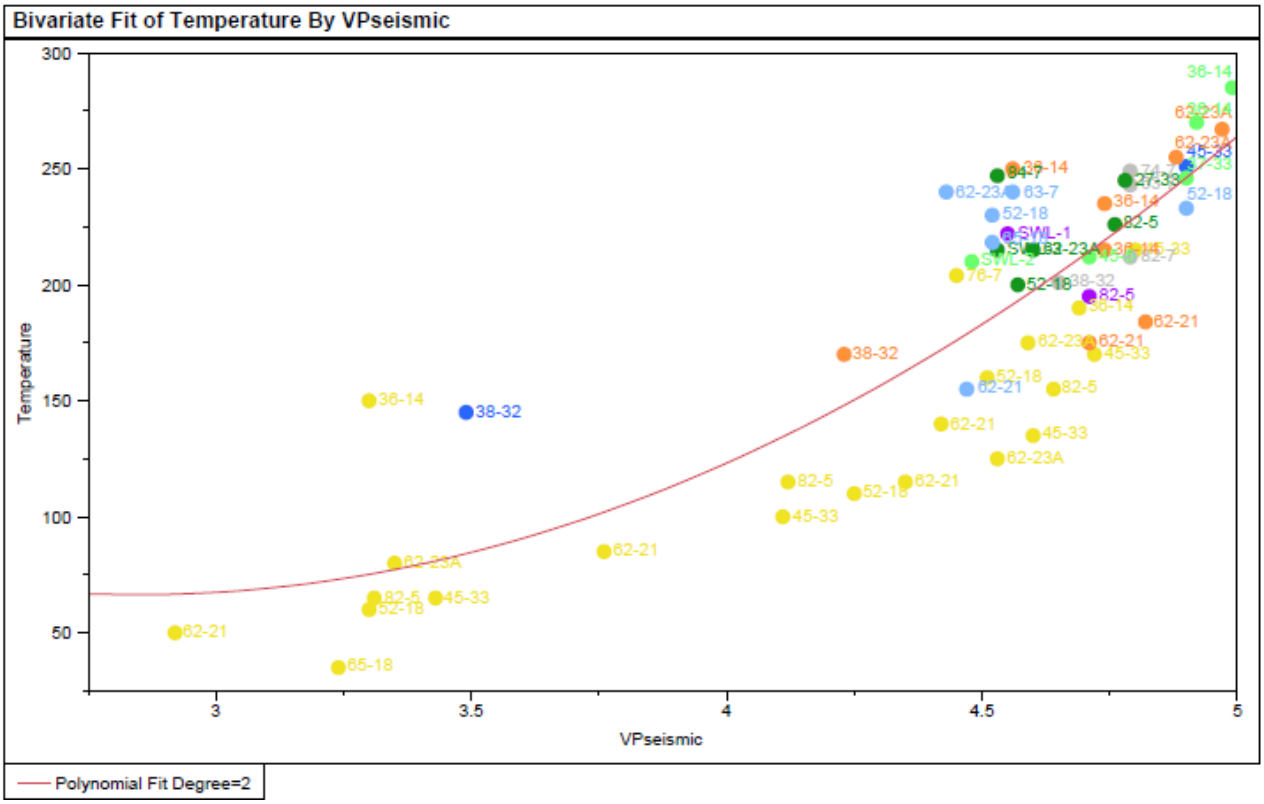

Figure 5: Modeled Vp vs. T using well data excluding data from +1km asl elevation and outlier wells (53-15, 66-21, 45-14 and 76-28) with a low seismic trust value. The polynomial fit has a R-square value of 0.72. The data is labeled by well name and color coded by stratigraphic formations: QTbf (yellow), Tmb (purple), Tv (dark green), Jz (light blue), Tr (orange), Kgr (light green) and Jbr (dark blue).

Bootstrapping with random sampling was used to estimate the precision of the R^2 reported above. The approximate 95% confidence intervals were calculated using 10,000 for each R^2 value. For the well data, R^2-values of 0.51 and 0.72, the 95% confidence interval was 0.36 and 0.65 and 0.54-0.83, respectively. These fairly wide confidence intervals are interpreted to result from the small sampling size of 76 for the R^2 of 0.51 and 55 for the R^2 of 0.72.

The above findings are empirically intriguing but it is recognized that vertical stress has a consistent positive relationship with Vp and T. The fact that all three parameters increase with depth may be the simple explanation for the aforementioned observations. We evaluated the well data result by multivariate analysis, dissecting the data by formation type, and by residual analysis (Iovenitti et al. 2012; 2013). Suffice it to report that the only link between the three parameters detected is depth which is most likely coincidental rather than a fundamental relationship between Vp and T. Nevertheless, the empirical relations should be examined at other B&R sites.

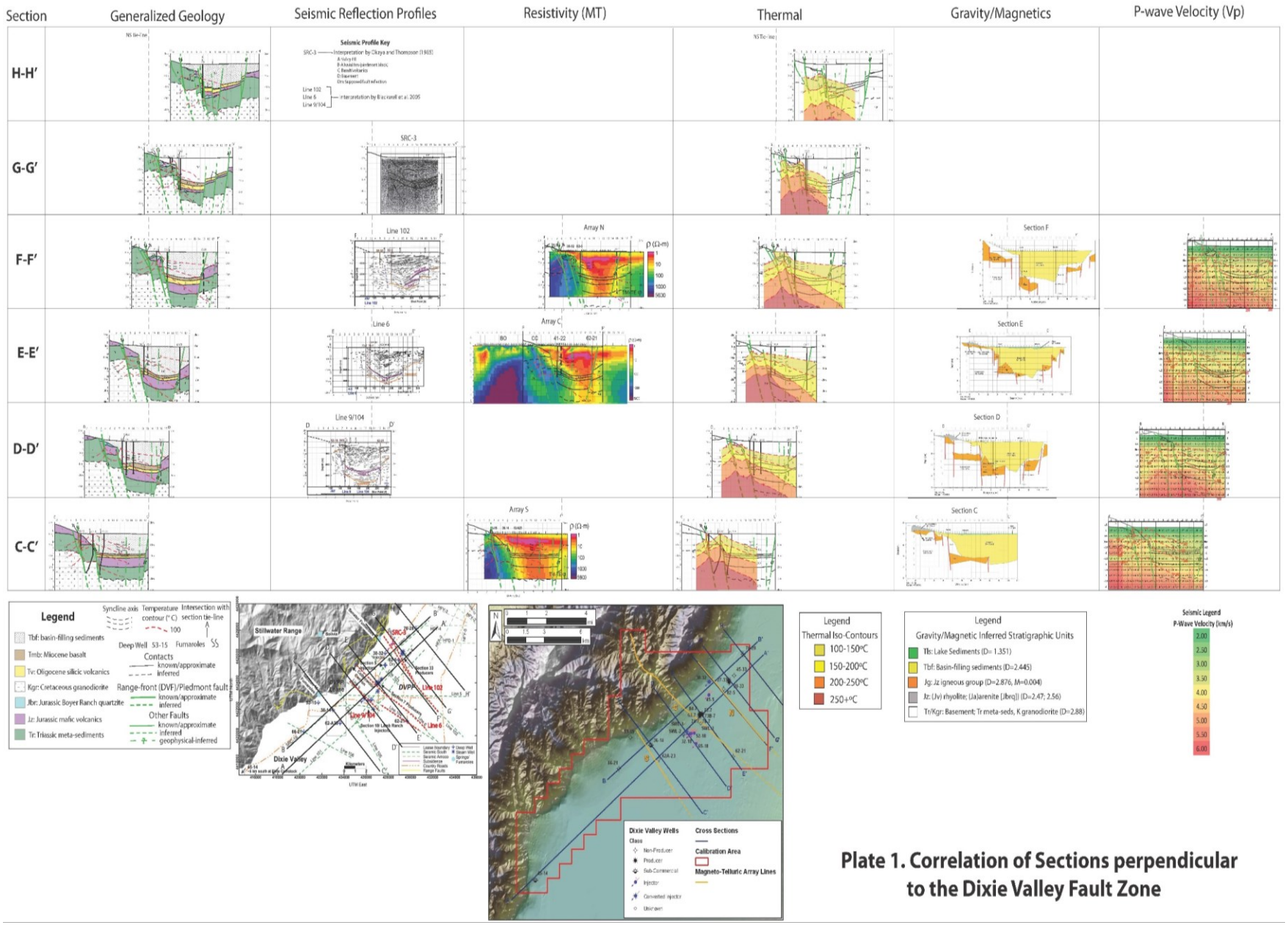

Plate 1. Correlation of Sections perpendicular to the Dixie Valley Fault Zone

2.2.3 Classification and Regression Tree Analysis

CART analysis was performed to determine which geoscience parameters may be a good predictor of EGS favorable conditions (i.e., T and lithology), expected EGS favorable cells and hydrothermal productive vs. non-productive cells using both the sectional and well data (Table 2). Explanatory variables used in this analysis were geoscience parameters with good qualitative and quantitative correlations and were used for response variable prediction purposes. These included: T, lithology type, gravity-magnetic inferred lithology, Vp, Coulomb Stress Change (CSC), dilatation, resistivity, and vertical stress. Table 2 presents the CART analysis R^2-values using all parameters as well as a sensitivity analysis when Vp is removed from the data set being considered. Example results analyses using sectional data (1) T can be predicted using all the variables with a R^2 of 0.87 and using dilatation only the R^2 is 0.68; (2) lithology can be predicted using all variables with a R^2 of 0.63 but could not be predicted when vertical stress was removed, $R^2 > 0.5$. Using the well data (1) T could be predicted using all the variables with a R^2 of 0.82, and using Vp alone, the R^2 is 0.62; (2) lithology can be predicted using all the variables with a R^2 of 0.61, using Vp and dilatation, the R^2 value is 0.55; (3) hydrothermal productive cells can be predicated using all the variables with a R^2 of 0.63, using Vp, lithology, and dilatation, the R^2 is 0.55; (4) expected EGS favorable cells can be predicated using all the variables with a R^2 of 0.73, using dilatation and lithology alone, the R^2 is 0.71.

2.3 Baseline Favorability/Trust Mapping

EGS favorability/trust maps at a grid scale of 0.5km by 0.5km for 0.5km incremental horizontal slices between +1km and -4k asl were made for the DVGW (i.e., the calibration area). The most important EGS parameters considered were in order of importance, T (above 200°C but less than 350°C), rock type or lithology (resistant, competent rock that can form fractures), and stress (extension being more favorable than compression). Four stress sub-parameters were considered (1) fault orientation, (2) presence or absence of a fault, (3) CSC, and (4) occurrence of a structural zone including compression, dilatation, or neither. Subject Matter Experts on the project team were polled to determine the relative favorability values of the individual parameters considered and the final weighting used in calculating EGS favorability values. Equal and average (based on Subject Matter Expert opinions) weighting factors were generated. Presented herein are the average weights for T, lithology and stress parameter weighting factors of 0.51, 0.30 and 0.20, respectively. Favorability weights and values used are presented in Table 3. Favorability values were calculated using the following equation:

$$F_v = (d_0 * w_0) + (d_1 * w_1) + \ldots (d_n * w_n)$$

where F_v is the favorability value for a grid cell, d_0 through d_n is the favorability value of a cell's geoscience parameter data, and w is the weight for a particular dataset.

Final baseline EGS favorability maps were visualized using GIS software. Only one potential realization is presented. Complementary depth trust maps were also generated to reflect underlying data reliability. Trust weights range from: hard data (i.e., from wells) with a weight of 5, to modeled data to inferred with weights ranging from 4 to 2 depending on Subject Matter Expertise data confidence, to no data with a weight of 1. An example coupled favorability/trust map at 3km below sea level (4km depth) is presented in Figure 6.

Table 3: Parametes for EGS favorability mapping, their values ranging from 1-9 (highlighted in yellow), and weights which sum to 1.

Temp.[1] (0.50 w[1])		Lithology[2] (0.30 w)		Stress Sub-parameters (.20 w)							
				Compression / Dilation Zone (.05 w)		*Fault Orientation (.05 w)*		*Structure Present (.05 w)*		*Coulomb Stress Change (.05 w)*	
100	1	QTbf	1	Compression	4	30-60°	7	Structure	7	< -22	2
125	2	Tmb	5	Dilation	7	Other	4	None	5	-22	3
150	2	Jz	7	Neither	5	Neither	5			-14	3
175	4	Tr	3							-6	4
200	7	Kgr	9							0	5
225	7	Tv	3							6	6
250	8	Jbr	8							14	7
275	9									22	8
300	8									> 22	9
325	7										
350	5										
> 374	3										

[1] Temperature in °C

[2] Represented by the generalized formations in Dixie Valley

Table 2: CART results including a sensitivity analysis sectional and well data. The first row for each prediction corresponds to R^2-value ranges with vertical stress considered, while the following rows, highlighted in green, show the R^2-values when vertical stress is removed from the analysis; see the text for a discussion.

Range of r^2-values from CART Sensitivity Analysis

Response Variable Prediction	Data Type	Explanatory Variables Removed from Analysis							Explanatory Variables in the Analysis Used when Vertical Stress Is Removed
		0	1	2	3	4	5	6	
Temperature	Section	0.871	.729 - .918	.727 - .918	.847 - .907	.735 - .898	.310 - .901	0.874	
Temperature (Vertical Stress is removed from consideration)			0.677						Vp, Resistivity (MT), and Gravity-Magnetic (G-M) Lithology
				0.806					Vp, Resistivity (MT), and G-M Lithology
					0.792				Vp, Resistivity (MT), and Dilatation
						0.885			Vp, Dilatation, and Lithology
							0.775		Vp, and Resistivity (MT)
								0.684	Dilatation
								0.359	Vp
Lithology		0.631	.627 - .655	.541 - .653	.523 - .665	.484 - .660	.505 - .656	0.507	
Lithology (Vertical Stress is removed from consideration)			0.438						Vp, Resistivity (MT), Dilatation, and G-M Lithology
				0.453					Vp, Resistivity (MT), Dilatation, and Temperature
					0.433				Vp, Resistivity (MT), Dilatation, and G-M Lithology
						0.421			Vp, Dilatation, and G-M Lithology
							0.406		Vp, and Dilatation
								0.277	Dilatation
Temperature	Well	0.822	.769- .841	.749- .841	.749 - .822	.749 - .805	.749 - .803	0.749	
Temperature (Vertical Stress is removed from consideration)			0.750						Vp, Resistivity (MT), CSC, Dilatation, and Lithology
				0.767					Vp, Resistivity (MT), CSC, Dilatation, and G-M Lithology
					0.775				Vp, CSC, Dilatation, and G-M Lithology
						0.730			Vp, Dilatation, and Lithology
							0.680		Vp and Lithology
								0.621	Vp
Lithology		0.611	.577 - .611	.562 - .611	.562 - .644	.562 - .620	.552 - .615	0.552	
Lithology (Vertical Stress is removed from consideration)			0.521						Vp, Resistivity (MT), CSC, and G-M Lithology
				0.529					Vp, Resistivity (MT), CSC, and G-M Lithology
					0.600				Vp, CSC, and G-M Lithology
						0.549			Vp, Dilatation, and Temperature
							0.550		Vp and Dilatation
								0.408	Vp
Productive vs. Non-productive cells		0.625	.447 - .617	.431 - .647	.523 - .665	.361 - .648	.315 - .587	0.389	
Productive vs. Non-productive Cells (Vertical Stress is removed from consideration)			0.528						Vp, Resistivity (MT), and Lithology
				0.615					Vp, Resistivity (MT), Lithology, and Dilatation
					0.433				Vp, Resistivity (MT), Dilatation, and G-M Lithology
						0.598			Vp, Lithology, and Dilatation
							0.550		Vp and Lithology
								0.457	Lithology
Expected EGS favorable cells		0.727	.523-.727	.383-.727	.409-.708	.369-.661	.349-.637	0.398	
EGS favorable cells (Vertical Stress is removed from consideration)			0.769						Temperature, Vp, CSC, Dilatation, and Resistivity (MT)
				0.769					Temperature, Vp, CSC, Dilatation, and Resistivity (MT)
					0.769				Temperature, Vp, CSC and Dilatation
						0.708			Temperature, Dilatation, and Lithology
							0.708		Dilatation and Lithology
								0.398	Dilatation

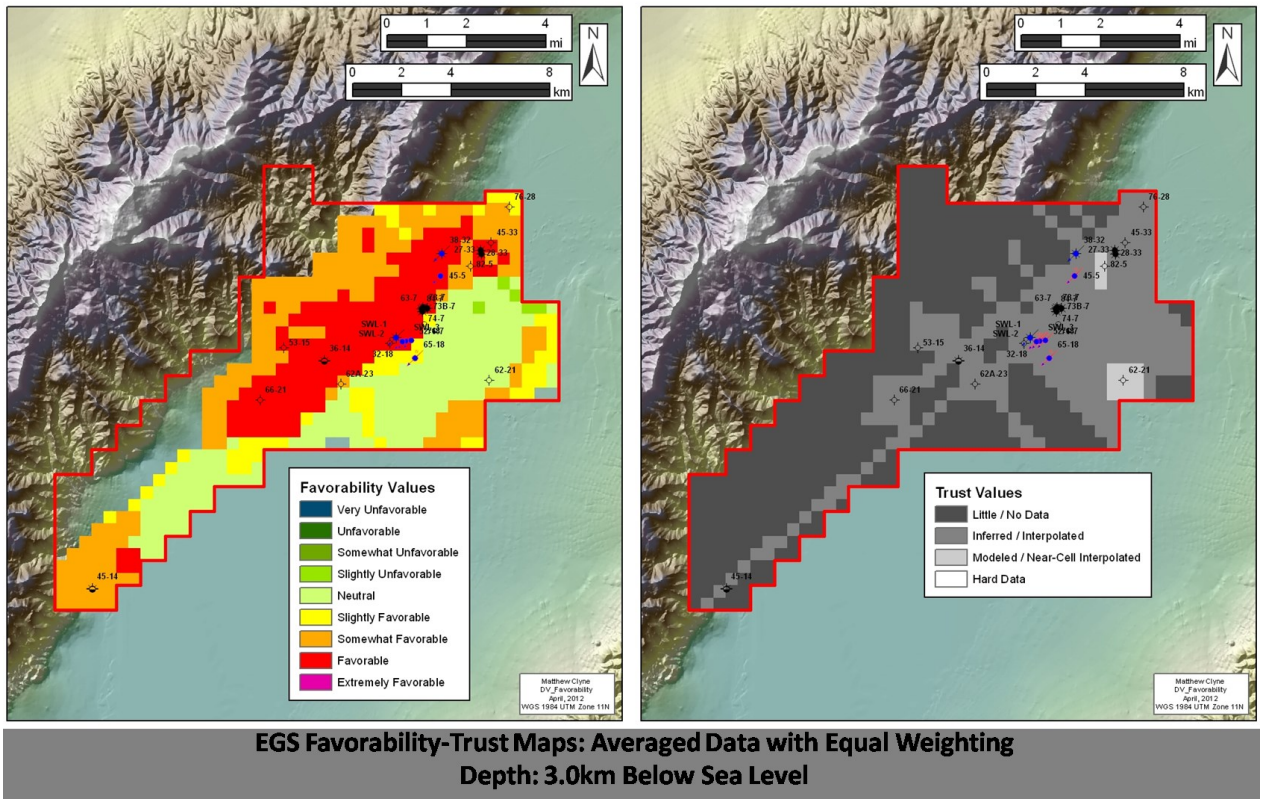

Figure 6: EGS favorability/trust maps at 3km below sea level (4km depth); the calibration area is outline din red.

3. ENHANCED INVESTIGATION

To reduce uncertainty, non-uniqueness and improve model resolution new geophysical and geochemical data were collected (1) 278 gravity stations, (2) 42 ambient seismic noise stations, (3) 70 new MT stations, and (4) 308 new soil CO_2 gas stations. Additionally, 3D conductive and convective thermal modeling was conducted. The soil gas survey resulted in a null results and will not be discussed herein.

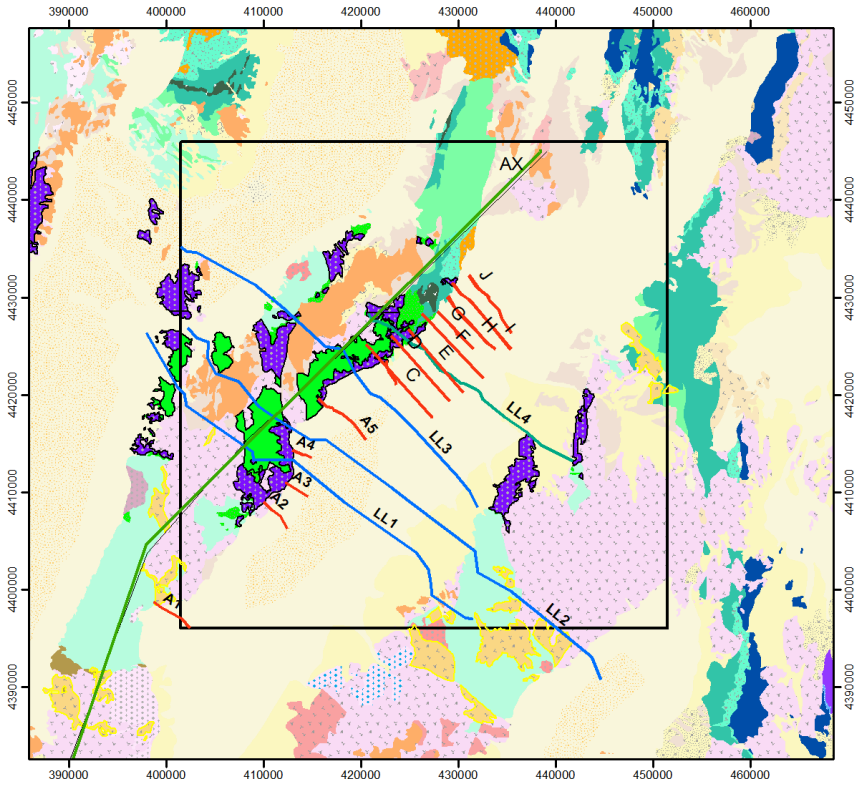

Figure 7: Gravity-magnetic profiles for the project area. The geologic base map is comparable to that shown in Figure 2.

3.1 Gravity-Magnetics

The objective of the new gravity stations was to fill in data gaps and expand the modeling efforts outside of the wellfield. Joint 2 ¾-D forward modeling of the enhanced (baseline + new) gravity and (baseline) magnetic data on 15 profiles (cross-sections) in the project area to determine subsurface structure and faulting (Figure 7). In general, fits of 1-3% precision were achievable for area models. In some cases it was necessary to model off-axis magnetic features. Each line showed minor scatter of up to 2-3mgal off a smoothed curve. The bedrock and basin was modeled with a density contrast of ~0.4gm/cc. The profiles were profiles in two ways (1) using basement D= 2.876gm/cc and fill D= 2.445gm/cc and (2) using bedrock D= 2.67gm/cc and basin-fill inverted for best fit. The two methods yielded similar results, verifying that the density contrast was the most important factor. In the magnetics modeling, a susceptibility of S = 0.007 (cgs) for Jg and Jv (herein called Jz) rocks and S=0.0 for all other units. This is equivalent to a magnetization of M= ~0.0035 emu/gm.

Both complete bouguer anomaly and residual gravity anomaly (CBA and RGA, respectively) profiles were evaluated and found in ground agreement (Figure 8). Good agreement was found when these results were compared with the seismic reflection lines (Plate 1) and mapped faults (Figure 2). A range of magnetic susceptibility (S) values were tested, S=0.002-0.21cgs to evaluate the effect of this parameter on the modeling results. For each of the profiles modeled, as S is increased, the location of the magnetic bodies remains the same, but the thickness of the bodies decrease particularly from the lower boundary. This implies that changing the magnetization does not significantly affect the positions of inferred faults reported, although the dips of the faults may not be as well constrained. The model results were very useful in defining basin structure delineating major and lesser bedrock faulting.

3.2 Ambient Seismic Noise Survey

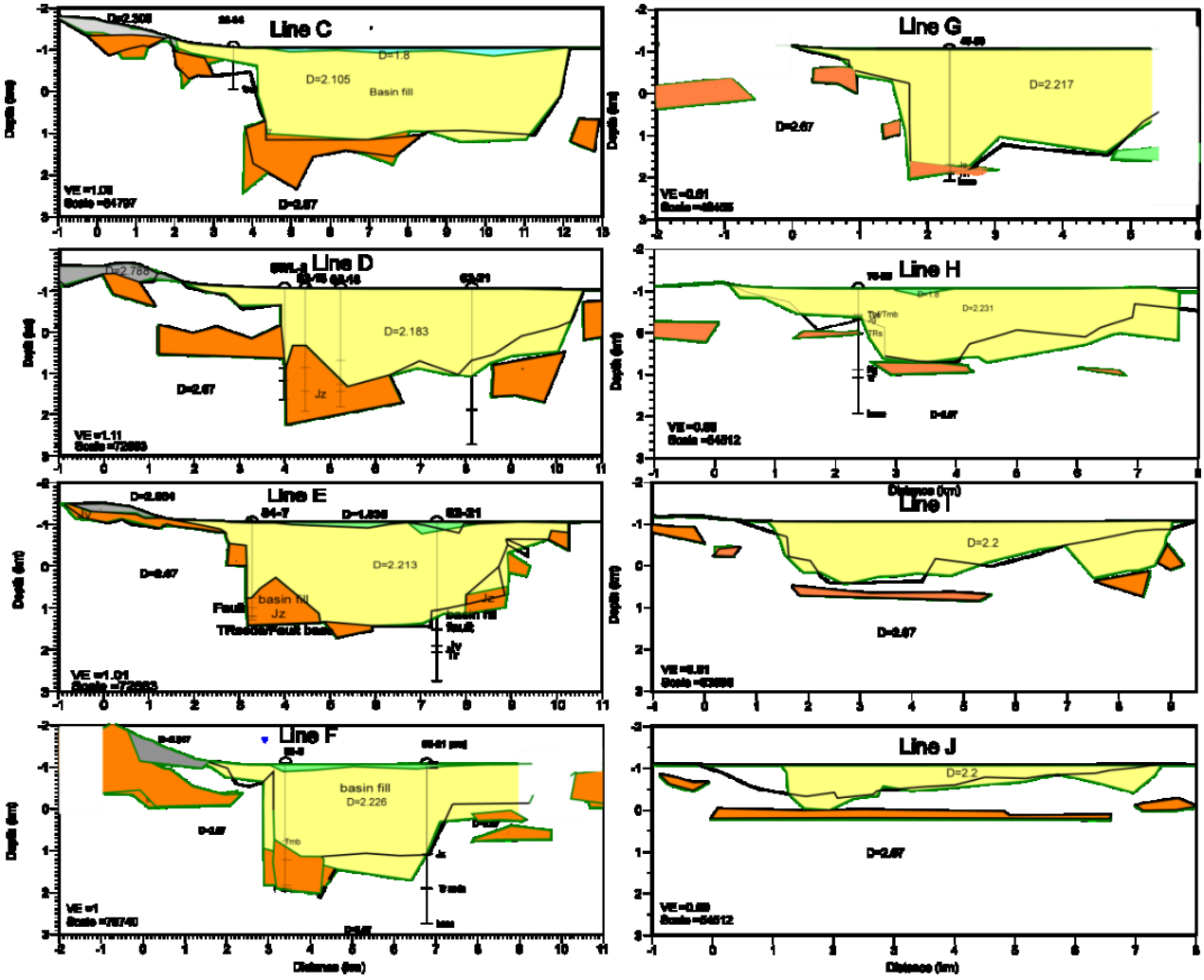

Figure 8: Select Complete Bouguer and Residual Gravity Anomalies (CBA and RGA, respectively) models of section lines in the project area. CBA models (filled solids with green outlines) and RGA models (black outlines)

To image the subsurface project area, an ambient seismic noise (ASN) array (21 three-component, broadband sensors, with an overall array aperture of 45km) was installed in two deployments, each with three-month duration (Figure 9). The ASN survey overall goal was to determine if seismic data could predict T and lithology using complementary information derived from regional tomographic models of body, shear and surface waves statistically integrated with

shear velocity models. Two objectives of this work was to estimate a high resolution (~5km^2) Vp and Vs velocity model in the project area using the enhanced data and other independent sources and extract maximum information in the calibration area (Figure 1). Seismic tomography practices required the use of an area greater than the project area to develop the tomographic model. This a larger region is referred to as the Dixie Valley Extended Study Area (DVESA), Figure 10.

Because T and rock type were not directly measured by geophysical methods they had to be inferred. Seismic methods directly measured velocity, which is affected by T, however, velocity is also affected by numerous other factors including fluid conditions and fractures, lithostatic pressure and rock type. Comparison of velocity anomalies with mapped and suspected rock types from other geophysical techniques may identify regions where velocity anomalies are not explained by petrology, and thus are more likely to be due to anomalous T. The seismic results were integrated with other geoscience data to infer T and rock type. New velocity models were estimated at three different scales ranging from hundreds of km to km, in the Dixie Valley region. At each scale, the new models had at least a factor of two improved resolution when compared to the baseline models.

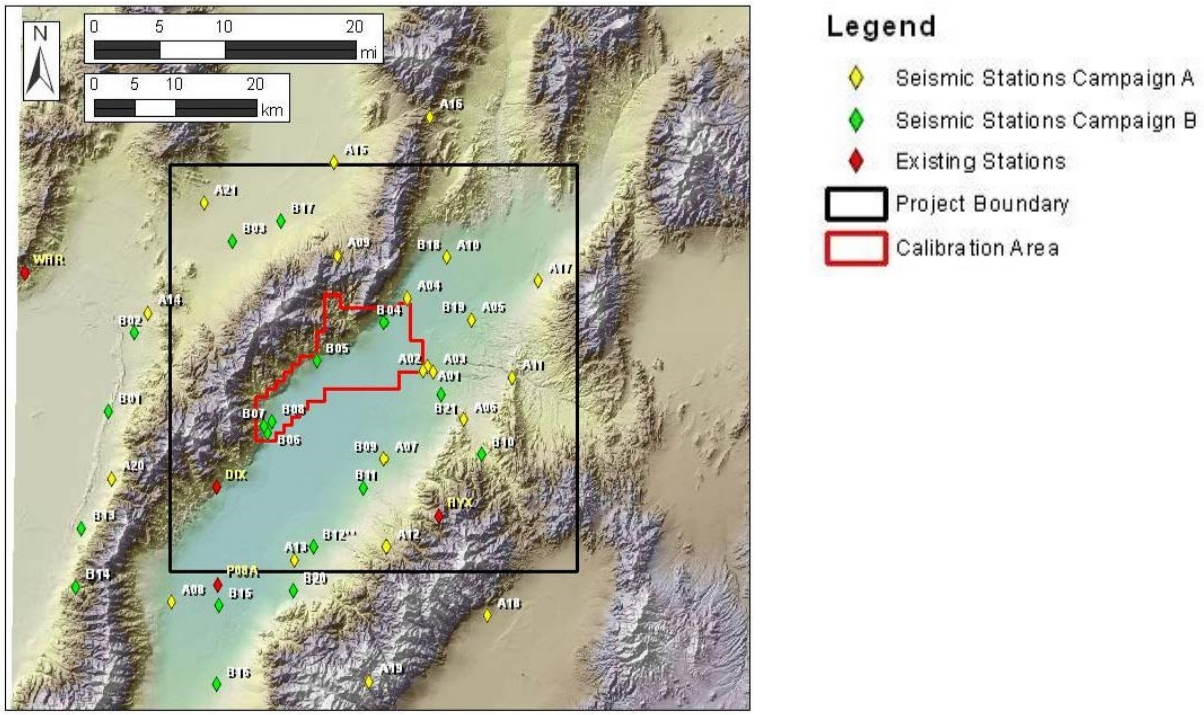

Figure 9: Ambient noise seismic survey station locations. Project area is the black box and the calibration area is outlined in red. The two seismic campaigns each were of 3-month duration.

At the DVESA scale, the project area occurs at the intersection of two different velocity model trends (1) an E-W low velocity corridor in the upper crust (less than 10km depth), and (2) a NW-SE low-velocity corridor at depths from 10km to 20km. The E-W low-velocity trend in the upper crust corresponds to the ~ 180km E-W extension along the 40'th parallel during the middle Miocene and Holocene (Bogen and Cshwieckert, 1985). The NW-SE low-velocity trend corresponds to an earlier extension, in the late Eocene-Oligocene (McKee and Moring, 1996). The intersection of the upper and lower crustal trends under the project area may explain the complex system of faults underlying it and a region of elevated crustal T suggested by a pronounced low velocity in the southwestern portion of the area and thermal data. At this intersection, low velocity anomalies start in the lower crust beneath Fairview Peak, "raising" from SW to NW within the mid-crust, and breaking up in narrower "conduits" at the upper crust.

At the project area scale, the highest velocity gradients appeared to follow faults. Low-velocity areas correlated (at least at the shallowest depths) with heat flow anomalies and low velocity areas are observed in the vicinity of the geothermal power plant. The project area velocity model was interpreted as indicating a close relationship between the high T (shown by low velocity) in the lower crust and the DVGW in the upper crust. The "hottest" lower crustal area southwest of the project area in the lower crust, and the low velocity appears to ascend from a SW-NE direction and peak in the DVGW, where 285^{o}C has been measured at ~3km depth in well 36-14. The existence of a highly fractured upper crust overlying a hot lower crust may be a possible cause of elevated high heat flow in the region. The production area in the DVGW is located on known faults some of which are delineated using high seismic velocity gradients.

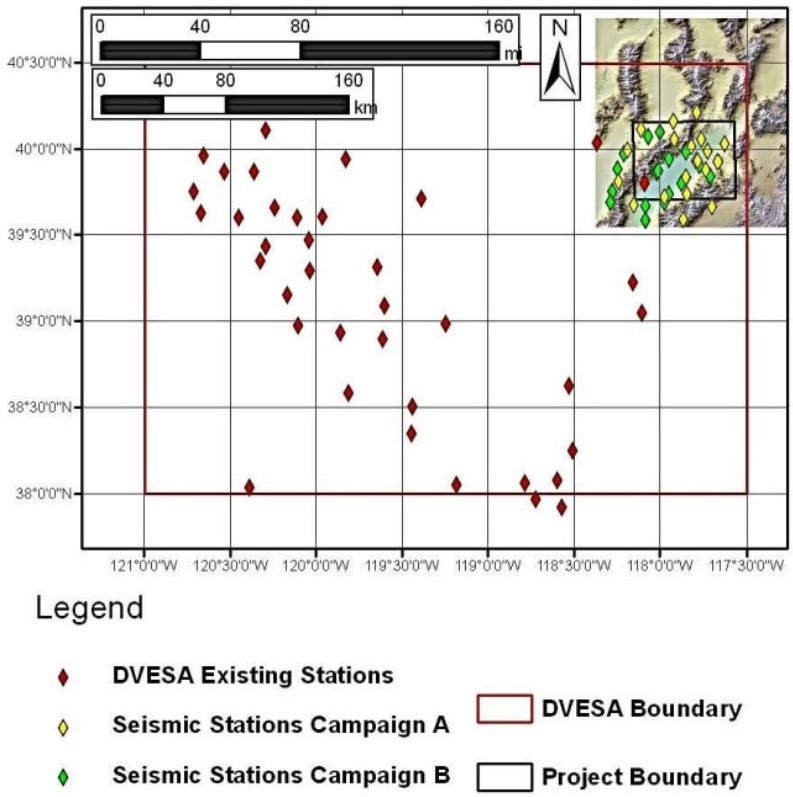

Figure 10: Seismic station locations used in the evaluation of the DVESA; see text for an explanation. The project area is shown in the upper right-hand (refer to Figure 9 for an explanation).

Although the Vs model velocity resolution (~5km) was lower than the Vp velocity model resolution (~3km) in the DVGW, and much lower than the comparable resolution (~0.5km) for other geoscience datasets reported herein, first order seismic velocity, density and attenuation values were associated with lithologic layers in Dixie Valley. Calculated velocity gradients with T, and velocity gradients with pressure in each well found them larger than the common crustal values. Positive variations of the seismic velocity with T, more pronounced for Vp than for Vs, were estimated from well data in the upper 3km supporting the baseline geostatistical analysis (see Section 2.2.2). These variations are contrary to laboratory experiments which predict negative velocity gradients with T increase, all other conditions being constant. The current results are interpreted as evidence that lithology and pressure affect the velocity more than the T increase and or porosity in the upper 3km. This interpretation may change as higher resolution velocity models are developed. Because Vs seemed to be affected by T and porosity more than Vp, the Vp/Vs variations with T appeared to be best correlated to the T-depth variations at well locations. Calculated Vp/Vs and found a slight correlation of high Vp/Vs with high well T- gradients. With limited resolution above 1km depth, seismic velocity is approximately linearly correlated with T increasing in each well. This behavior is interpreted as dominant pressure (or porosity) effects within the upper 3km. Vp/Vs should increase with increasing T at the same pressure, however, some wells show decreases with increasing T. Causes for this behavior would be as pore pressure and lithology variations. Vp/Vs was also found, with one exception, to be lower in "cold" wells (T<200°C) than at the same depth in the high-T wells. Low Vp/Vs was in all cases observed at mid crustal depths (12-15km) at the "cold" wells.

3.3 Magnetotellurics

Seventy new tensor MT stations were taken and merged with 24 existing (baseline) soundings for a total of 94 sites (Figure 11) over the DVGS for development of an enhanced 3D MT interpretation (Wannamaker et al. 2013). At typical geothermal conditions, electrical resistivity in turn is controlled primarily by (1) the quantity, salinity and efficiency of long-range interconnection of aqueous fluids in pores and fractures, and (2) the presence of hydrothermal alteration mineralogy with appreciable cation exchange capacity (Palacky, 1987). Secondary controls on the resistivity of host rock lithologies include minor variations in porosity and clay content, most of which may predate geothermal activity of interest. The four complex elements of the multi-frequency impedance generated by the survey at each MT sounding were input to a non-linear (iterative), regularized inversion program to produce a 3D model of electrical resistivity under the Dixie Valley region with particular emphasis in the calibration area (Figure 11). The algorithm used is based on that described by Sasaki (2004). The 3D code used finite difference (FD) approximations to Maxwell's equations to simulate the MT response of the 3D earth and the sensitivities of the response to incremental changes in the resistivity of each parameter.

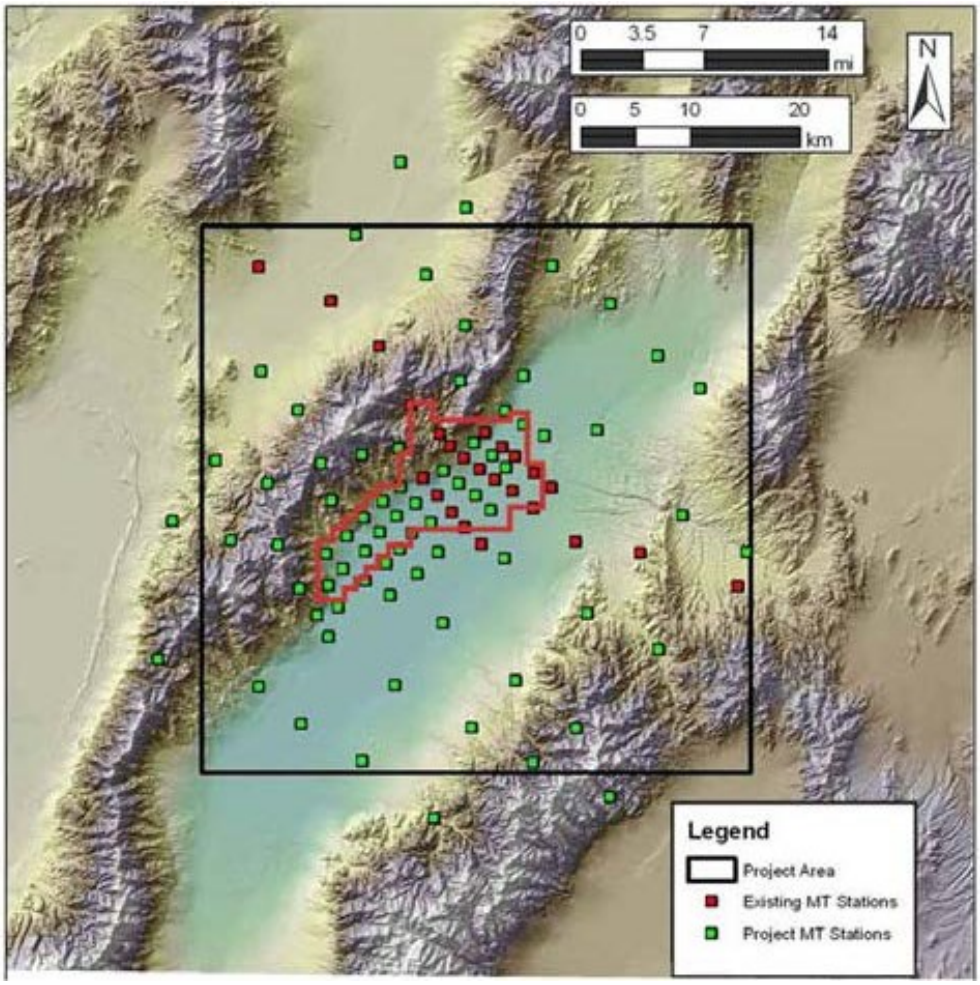

Figure 11: MT survey stations in the Project Area (black box); calibration area is outline din red.

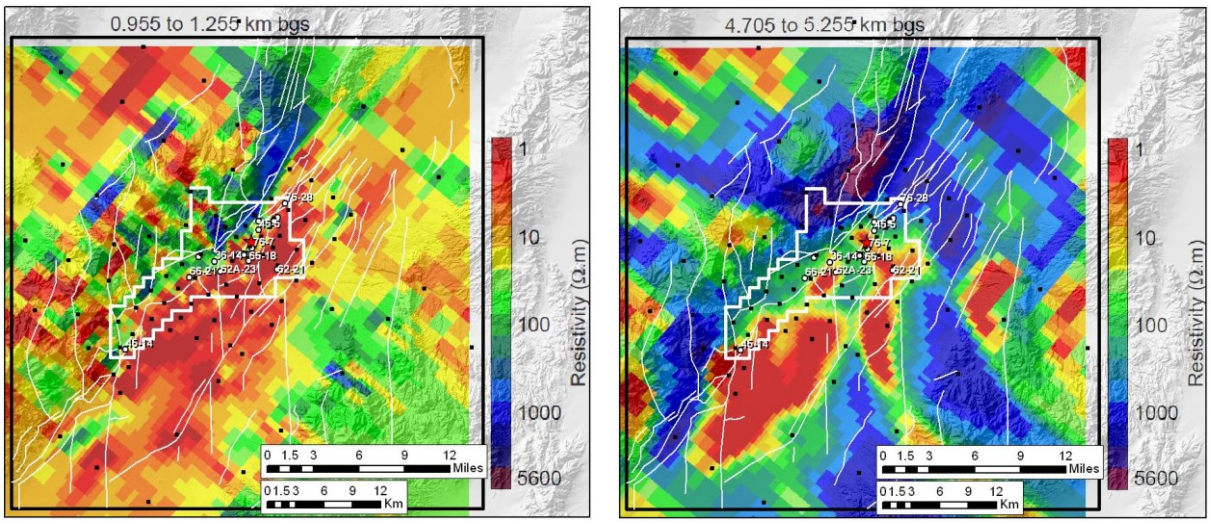

Figure 12: Select MT slices through the project area on about 1km (left) and 5km (right). Mapped faults in the project area are shown as thin white lines. The calibration area is outlined in bold while lines. The DVGW (see text for explanation) are indicated by white circles and the well IDs.

A series of MT depth slices were made through the project area along with a 3D perspective view from the surface to 20km (Wannamaker et al, 2013). Among the primary features observed in these data are:

1. The NE-SW trending current B&R structure can be seen in the MT slices from a depth of about 1km to about 3km (Figure 12 where some of the conductive elements begin to align N-S and NW-SE. This realignment of some of the low resistivity anomalies becomes more pronounced with depth.
2. The low resistivity, on the order of 1 Ω persists to depths >10km. This low resistivity has been postulated by Wannamaker et al. (2013) to be the result of a high T (based on depth of occurrence) saline aqueous fluids.

However, such fluids are not evidenced in the relatively shallow (<3km) current hydrothermal system generating electricity.

3. The MT structure shows evidence for the intersection of NE-SW and NNW-SSE regional structural trends considered critical to the localization of permeability in the geothermal system (Section 2.1).

3.4 Thermal Modeling

3.4.1 Conductive Model

Thakur et al. (2012) reported on the 3D conductive model for the project area (Figure 1). The thermal conductivity contrast between the basement/range and Q-Tb, and conductive heat transfer form the basis of the model. Heat flow values for ranges and valleys were averaged separately because of their difference in the topography and the geology. A gradient of 55^{o}CKm^{-1}was chosen to be the best value representing the purely conductive heat flow in the valley. Thermal conductivity measurements of various alluvium samples at shallow depth (<200m) yields thermal conductivity values from 1.41 to 1.5 Wm^{-1}K^{-1} with an average of 1.25Wm^{-1}K^{-1} (Blackwell et al., 1994). Background heat flow in the valley was calculated at 81 ± 3mWm^{-2}. The average thermal conductivity value for volcanic rocks and meta-sedimentary rocks was assumed to be 1.4 Wm^{-1}K^{-1} and 2.5 Wm^{-1}K^{-1}, respectively. The average heat flow in the ranges was considered to be 91 mWm^{-2}. Regional heat flow in the vicinity of Dixie Valley is 82 mWm^{-2}, which is close to the average heat flow of the Basin and Range region of 85-90 mWm^{-2} (Lachenbruch and Sass, 1977; Blackwell et al., 1991).

Major variations in heat flow and T in the project area result from (1) an ~1400m elevation difference causing topographic effects on the subsurface T and (2) the geometry of the ~2-3km thick valley fill causing the refraction of heat due to the thermal conductivity contrast between the valley fill and range/basement (a factor of 2). The vertical heat flow variations due to heat refraction are shown in Figure 13. Even though the basal heat flow is ~90 mWm^{-2}, the calculated heat flow varies from 60-120 mWm^{-2} within and around the valley.

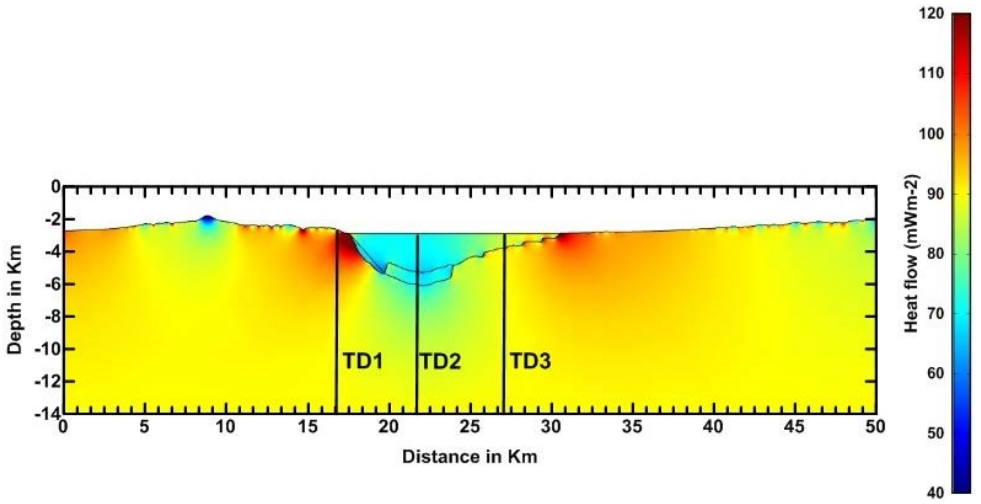

Figure 13: Heat flow variation resulting from thermal conductivity contracts between the valley fill (Q-Tb) and basement. Section runs NW to SE with the Stillwater Range on the left and the Clan Alpine Range on the right (see Figure 1). Note region of high heat flow on the NW-side of the valley corresponds to the DVFZ.

Heat flow analysis with depth showed that in sedimentary basins such as Dixie Valley with depth of sedimentary fill ~ 3km and width ~15-20km, surrounded by basement rocks of high thermal conductivity, large heat refraction effects occur. Based on the 2D and 3D thermal models, the heat flow varies by 100% (~ 90 ± 30 mWm^{-2}) due to the shape of the basement and the thermal conductivity contrast. Wells drilled in the vicinity (~ 2-5km) of sedimentary basins edges, even in the absence of a geothermal anomaly will in general show variations in heat flow with depth. This behavior happens due to the fact that heat flow is focused along the edges of the basins; i.e., more heat is flowing than the background in the basement rocks near the edge of the basin. A maximum T of 248^{o}C was determined at a depth of 5km in Dixie Valley using a 3D conductive steady state model. Moderately high heat flow anomalies along the valley range contact can be due to refraction of heat flow and may not be associated with any hydrothermal system.

3.4.2 Pseudo-Convective Model

Initial considerations of a 3D convective model suggested issues with the lack of thermal data within the Stillwater Range. As a result, an approximation of the convective field for the calibration area (Figure 1) was developed and the approximation is referred to as the 3D pseudo-convective model.

Using all measured T data in wells available to the project, the T field was modeled along eight cross-sections within the wellfield considering the general hydrothermal model where there are two major thermal-bearing structures in the DVFZ and a fall-off in T toward the valley (Blackwell et al. 2005). Cross-sectional data was gridded within 500m by

500m cells and applied to the calibration area at various depths, by interpolating and extrapolating values in Microsoft EXCEL. This thermal model consisted (1) measured values, (2) modeled values along the major cross-sections, and (3) interpolated and extrapolated values which filled in missing areas in the calibration area within 1km of the cross-sectional or well data. It is comprised both the convective and conductive components of the system and is referred to as the overall T model (T*overall)*. The conductive T field determined by Thakur et al. (2012) was gridded in the same manner described above. By subtracting the expected T(*conductive)* component from the T(*overall*) model, a first approximation of the T(*convective)* component was derived.

Figure 14 presents this pseudo-convective model at a depth of -1km asl along with faults, shallow thermal anomalies, and the location of active fumaroles in the calibration area. Areas within the Stillwater Range and to the southwest of the producing field are not included in the model due to a lack of data. The model showed that (1) the area within the

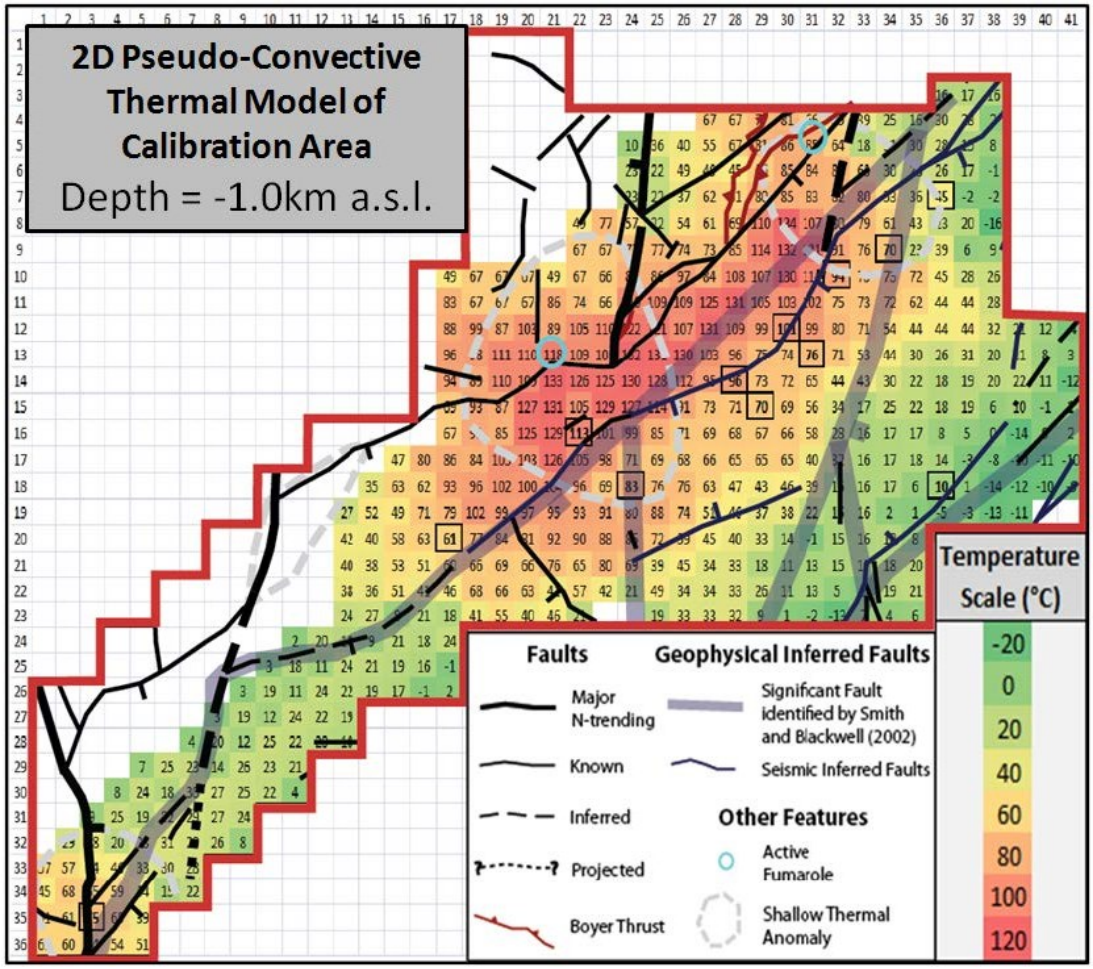

Figure 14: Pseudo-convective thermal model of the calibration area at a depth of -1km asl (2km below sea level).

DVFZ has elevated T as expected, (2) Ts fall-off and approximates the conductive regime both valley ward towards 62-21 and southwestward towards 45-14, and (3) the location of shallow thermal anomalies and fumaroles correlate with areas that show an elevated convective component. This pseudo-convective model provides a first estimation of the accuracy of the conductive model (Section 3.4.1). As such, areas of excess T considered resulting from convection may represent an exploitable hydrothermal system.

3.5 Enhanced Qualitative Geoscience Correlations

The enhanced data qualitative geoscience correlations are described below at three different scales: regional, project area, and calibration area.

3.5.1 Regional Scale

It is postulated a mid-crustal level low Vs anomaly identified in the DVESA may reflect magma under plating found at comparable depths by Wannamaker (2006) in the regional Great Basin MT transect slightly north of the region investigated herein. This postulation is further supported by (1) elevated excess He-isotopic data in the Dixie Valley (Kennedy and Soest, 2006), Soda Lake, and Brady's Hot Springs geothermal systems to the west of the project area (Hunt et al. 2011) may result from the interaction of deeply circulating meteoric water with mid-crustal depth magma, and (2) magmatic gases (N/Ar) in vein material fluid inclusions and production fluid from the DVGW by Lutz (2002). However, there is no evidence of magma contributing to the heat flow in the DVGS (AltaRock, 2014b). To explain

these limited observations, it is speculated that episodic release of mantle material to mid-crustal depths (as evidenced by the seismic and MT data) with accompanying fluid–rock interaction resulting in the elevated He and N/Ar ratios. This interaction however appears to add not significant heat to the overall systems. Additionally, the major seismic structural intersection at the southwestern portion of the project area (see Section 3.2) and N-S and NW-SE trending structures at depth (see Section 3.3) may facilitate communication fluid communication from the mid- to shallow-crust.

3.5.2 Project Area Scale

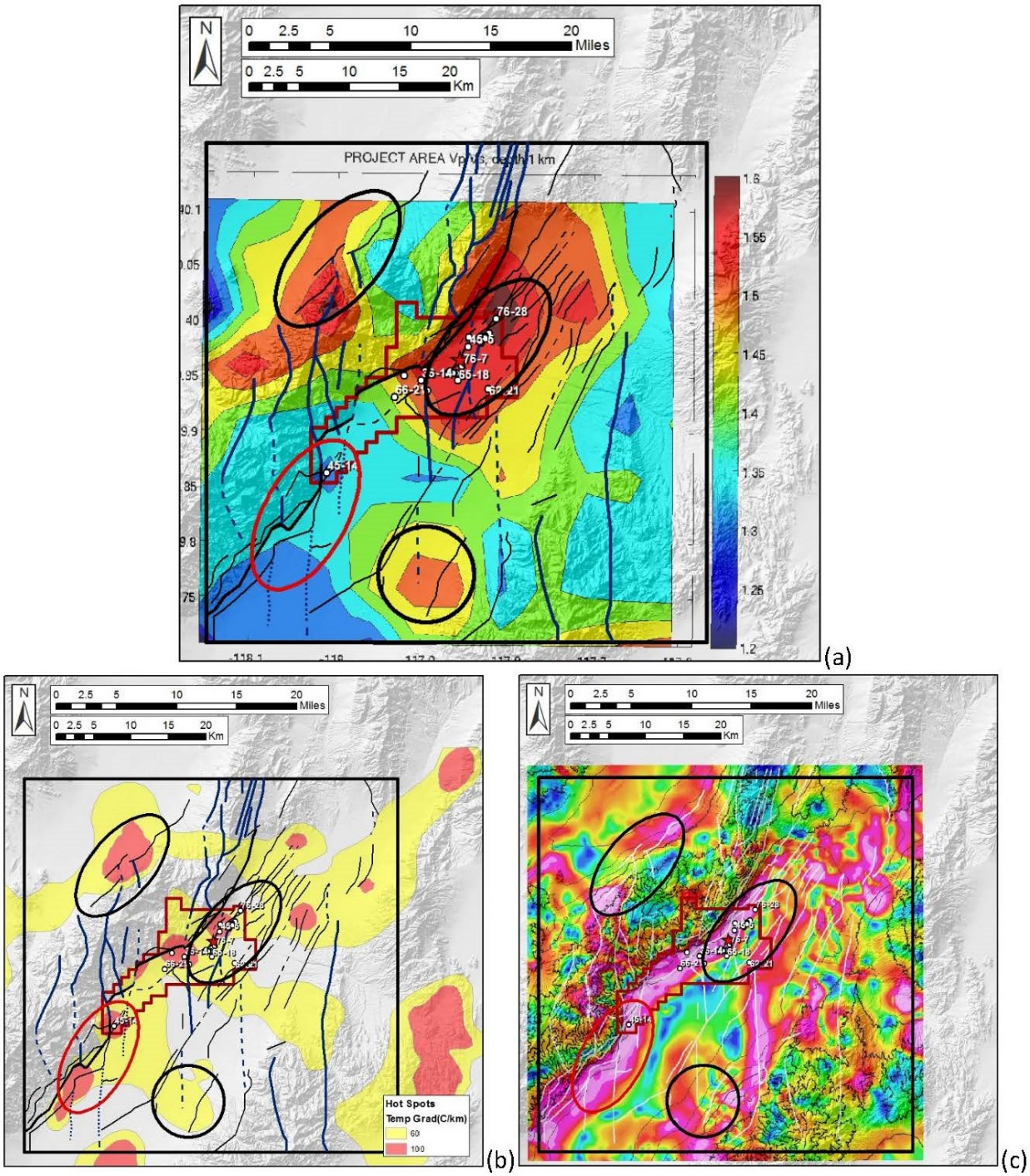

Figure 15: (a) Vp/Vs, (b) conductive geothermal gradients and (c) horizontal gravity gradients for the project area. Anomalies of higher Vp/Vs and conductive gradient are circled in black (hydrothermal favorable) and areas of lower Vp/Vs and higher conductive gradient are circled in red (EGS favorable).

Thermal effects on seismic velocities can be seen from the low seismic velocity anomaly in the project area at the DVESA scale. Slight seismic velocities variations from mean values within the project area may be used to infer various degrees of fracturing and fluid saturation at that scale. O'Connell and Budiansky (1974) proposed theoretical constraints on the effective elastic properties of rocks based on the presence of fractures and fracture density. Both the effective Vp and Vs decrease with increasing fracture density but at different rates, which causes Vp/Vs to increase in

saturated fractured rocks and decrease in dry fractured rocks. If the local mean values of Vp, Vs, and Vp/Vs are used to approximate the 'unfractured' values, then variations from the mean values can not only be used to infer degrees of fracturing locally, but can also be used to distinguish conventional geothermal resources from potential EGS areas when compared to local T anomaly maps (Figures 15 a and b). Higher Vp/Vs anomalies with high conductive geothermal gradients, such as in the northeastern part of the calibration area correspond to conventional geothermal reservoirs, whereas areas with lower Vp/Vs values and high gradients such as near well 45-14 in the southwestern part of that area may represent potential EGS favorable areas. Higher degrees of fractures can also be corroborated by the presence of large fault intersections that locally concentrate stress and increase fracture density as evidenced by surface mapping and at depth from horizontal gravity gradients (Figure 15c).

3.5.3 Calibration Area Scale

Five geoscientific data sets of varying quality and quantity available for the calibration area (Figure 1) were generated in this investigation: geology and well data, 2-3/4 gravity-magnetics model, 3D MT model, 3D seismic models, and thermal models. Additionally enhanced geoscience sections were prepared and gridded at 500m x 500m throughout the DVGW as in Plate 1. Major enhanced qualitative correlations, other than the geology and well data which was used for calibration purposes, are:

1. The gravity-magnetic model inferred lithology/structure model identified the major basin-fill/basement geometry and significant faulting. It accurately identified faults of significant offset as well as more minor faults, fault dips, and buried faults with no surface trace. Additionally, it identified major N-trending structures in the valley that have previously only been detected in certain seismic reflection lines and/or inferred on the basis of structural continuation from the range. It also found that the area of production/injection are generally associated with the gaps between magnetic Jz units which corresponds to identified dilatational zones. The modelingshowed, in the area of the DVFZ specifically between the range-front fault and piedmont fault, reduced thickness of the Jz unit or no magnetized Jz units. The magnetized Jz is apparently de-magnetized, not originally emplaced in this area (Jz is part of a thrust plate), or non-magnetic Jz units may be present.
2. The MT resistivity model identified the basin-fill/basement geometry, found basin-filling sediments as very conductive (1-10 ohm-m) when correlated with the geology and gravity-magnetics model, provided general correlation with major structures occur along maximum horizontal resistivity gradients between 500-1000m, identified the older N-trending faults and fault intersections occur as relatively low resistivity structures or areas of extreme low resistivity both laterally and vertically, identified active hydrothermal areas (both production and injection) generally correlate with moderate resistivity (~100 Ω-m) blocks along the hanging wall block of the piedmont fault but this correlation may not be unique, low resistivity (<10 Ω-m) observed in the MT data appears directly correlated in large part to the presence of N-trending faults, low resistivity (<10 Ω-m) zones generally extend to significant depths in the valley. It provided a very general impression of structure and it is non-unique with respect to the well data.
3. The seismic velocity models showed some correlations to structure as breaks in the velocity model coinciding with known faults, but this relationship is non-unique, possibly resulting from much greater, ~5km model resolution.
4. The pseudo-convective thermal model showed areas of excess convection suggesting the presence of a hydrothermal system.

3.6 Enhanced Quantitative Geoscience Correlations

Bivariate analysis showed that T is weakly correlated with all geoscience variables (depth, CSC, dilatation, Vp, Vs, and resistivity), except for Vp and Vs. Due to the strong relationship between T and depth along with many of the variables with depth, an approach was used to control the effect of depth to predict T using (1) residuals as a dependent variable in multiple regression and (2) the difference between each T and the average T at that depth in the calibration area.

Using multiple regression analysis in predicting T the best fit with two variables was Vp and CSC, giving an R^2 of 0.659. With all variables except for Vp, R^2 is 0.659. With Vp and depth omitted (leaving CSC, dilatation, Vs and resistivity), R^2 decreases to 0.501. Dropping depth and both Vp and Vs (since both are highly correlated with depth), reduces R^2 to, 0.046 (using only CSC, dilatation and resistivity). This drastic reduction in R^2 identifies depth as a powerful confounding but a significant contributing factor. Consequently, the next phase of the analysis focused on the relationship between Vp and T independent of depth was to predict T based on depth and used the residuals as a dependent variable in multiple regression. The R^2 for the T residuals in the multiple regression analysis was 0.091, in spite of the fact that the large number of observations results in highly statistically significant1 predictors such as dilatation. The results (correlations between T-Differences and other variables, and summary of fit) were very similar to the analogous results using T- Residuals. Using multiple regression with all seven variables (including depth) to predict the T- Differences gave an R^2 of 0.062.

As in the baseline model analysis, CART was used to model the ability of the geoscience variables to predict several variables of interest. In addition to predicting T and whether grid cells would be productive for hydrothermal or

inferred EGS, we also predicted T-Residuals. The basic results for the enhanced CART analysis are summarized in Table 3. The ability to predict T, R^2 of 0.74, is fairly similar to the baseline analysis (Table 2).

Table 3: Summary of Enhanced CART Analysis

Response Variable Prediction	Selected Geoscience Variables Considered (x) and Used (X)						R^2 value
	T	*Vp*	*Vs*	*Coulomb Stress Change*	*Dilatation*	*Graviry-Magnetic Lithology*	
Temperature	---	X	X	x	x	X	0.74
T-Residuals	---	X	x	x	x	x	0.38
Predictive Productive Hydrothermal Grid Cells	X	X	X	X	X	x	0.19
Predicting inferred EGS Grid Cells	X	X	X	X	X	x	0.15

The low R^2 value for predicting productive hydrothermal and inferred EGS cells was not a particularly good indication of the success of this method because of the sparseness of favorable cells. Only 18 cells out of 4297 cells (with no variables missing) were productive hydrothermal, and only 21 were inferred EGS favorable. Perhaps a more appropriate way of looking at this result is that we are looking for a "needle in a haystack". CART cannot explain a very high proportion of the variability in the predicted variable (i.e., the R^2 value), but it did do a reasonable job of reducing the size of the "data" haystack searched as discussed below.

Figures 16 and 17 present the trees corresponding to the fewest variables that still achieved the maximum observed R^2 value for hydrothermal and EGS favorable cells, respectively. The tree for productive hydrothermal cells (Figure 16) had three terminal nodes worth examination. In the figure these nodes have the number of cells displayed in blue and in a slightly larger font.

1. *For Dilatation* >-1.49 x10-6, CSC <-23.5, Vp <5.26, and resistivity (MT) >108.5, three out of six cells are productive hydrothermal.
2. *For Dilatation* between 3.58 x 10-6 and 3.75 x10-6, and CSC >18.5, two out of five cells are productive hydrothermal.
3. *For Dilatation* between -1.49 x10-6 and 3.58 x 10-6, CSC between 18.5 and 24.5, and Vp between 4.41 and 5.27, four out of eight cells are productive hydrothermal.

Taking these three nodes together, CART identified 19 cells that seemed to have characteristics that make them likely to be productive hydrothermal, and 9 of these cells actually are. Although the R^2 value is not very impressive, CART has managed to reduce the size of the "data" haystack from over 4000 cells to 19, of which nearly half are productive hydrothermal.

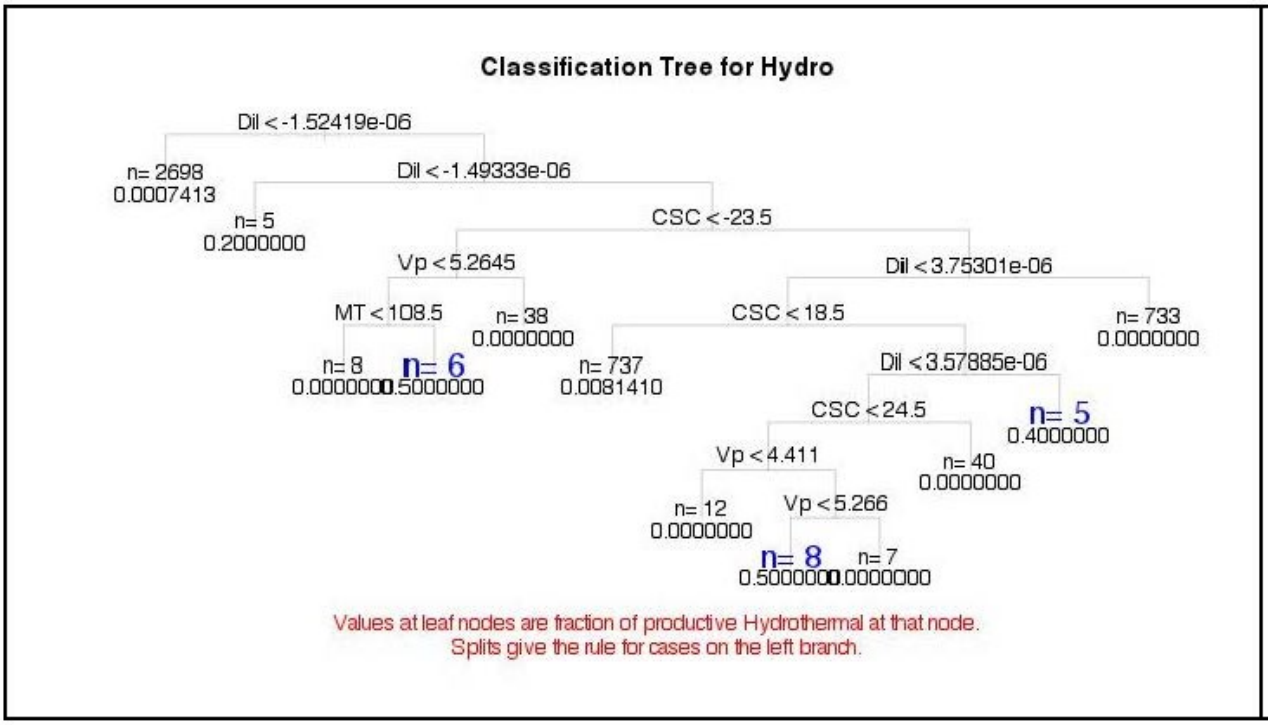

Figure 16: Select portion of the CART analysis for productive hydrothermal grid cells; see text for explanation.

For the EGS tree (Figure 17), there are two nodes with a substantial proportion of inferred EGS cells. These nodes have the number of cells displayed in blue and in a slightly larger font.

1. *For Vp* <5.63, T >239.5, and Dilatation >1.39 x 10-6, three out of eight cells are inferred EGS.
2. *For Vp* < 5.63, Temp between 197.5 and 239.5, MT between 37.5 and 40.5, and
3. *For Dilatation*, > -8.99 x 10-7, three out of five cells are inferred EGS.

For these two nodes, we have a similar reduction in the "data" haystack size as in Figure 16 from over 4000 cells to 13 cells of which six are Inferred EGS favorable cells.

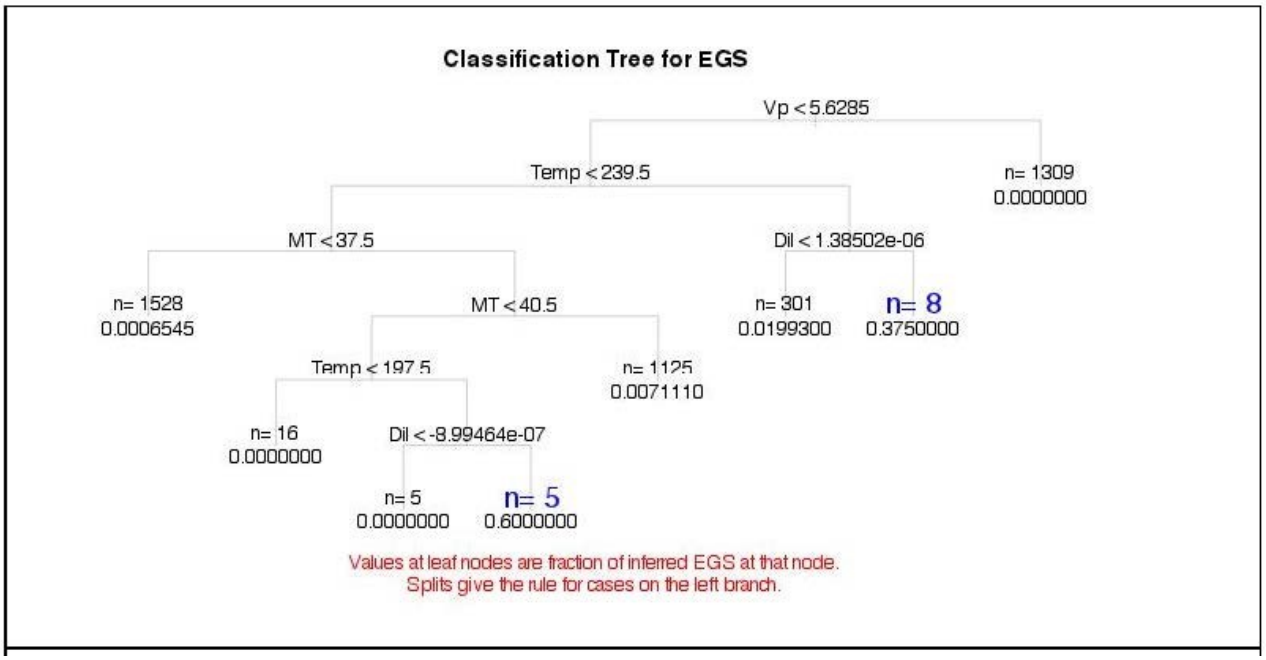

Figure 17: Select portion of the CART analysis for inferred EGS favorable grid cells; see text for explanation.

3.7 Enhanced Favorability/Trust Maps

The generation of the favorability maps for the calibration area (Figure 1) are based on three critical EGS geoscience parameters: T, rock type, and stress. The enhanced thermal data, conductive thermal modeling for the project area, convective modeling of the Dixie Valley Fault Zone (DVFZ), and pseudo-convective modeling, provided a variety of new insights into the thermal setting of the DVGS, but it did not provide new T data that would supersede the T data used in the baseline mapping discussed In Section 2.3. The enhanced seismic data analysis did develop an interesting prediction of T at depth. However, the methodology is new and not validated at other sites. As such, it was not used to supersede the baseline thermal data. Finally, while new earthquakes were detected in the project area during the deployment of the ASN survey and sufficient microseismic data was generated to allow inversion for stress, there was insufficient budget to analyze the data. As such, no new stress data was generated. The enhanced data did provide a greater confidence in the integrated interpretation of the geothermal setting of the calibration area but this was not sufficient to generate new trust maps. Thus, new enhanced favorability/trust maps were not generated.

5. Conclusions

Both public domain (baseline data) and new geoscience (enhanced) data generated in this project on the Dixie Valley geothermal system and its surrounding area were evaluated to determine which exploration tools were useful for defining EGS drilling targets. In this process, aspects of the hydrothermal system was examined. Both geoscience data were interpreted and integrated into conceptual models at a grid-scale scale of 0.5km x 0.5kmx two-dimensional cross-sections and in slices from +1km asl to -4km asl in 0.5km increments. Both datasets were also evaluated geostatistically evaluated at the same grid scale. EGS favorability/trust maps based on the three key EGS parameters or rock type, lithology and stress were also generated.

Stratigraphy and structure were found to be fundamental in understanding the geologic setting along with gravity and magnetic modeling. MT in this B&R geothermal stetting was useful for general structural trends and collaborating the general structural setting identified by structural and combined gravity-magnetics analysis. A new seismic technique, ambient seismic noise provided regional geophysical setting insights and a promising method was developed to predict temperature and lithology at depth. Vp/Vs was also found, with one exception, to be lower in "cold" wells (T<200°C) than at the same depth in the high-T wells. Low Vp/Vs was in all cases observed at mid crustal depths (12-15km) at the "cold" wells. Additionally a new promising method was developed for prediction of temperature and lithology using seismic data which is recommended for further evaluation and validation. An empirical T-Vp relationship where, as T increases the Vp increases, was identified but the relationship was not sustained when the

effect of depth was removed. Baseline CART analysis identified potential relationships between some geoscience parameters analyzed the ability of the data to predict T, lithology, productive hydrothermal grid cells and inferred EGS grid cells. However, these relationships were not detected in the enhanced dataset and this may be explained by the "needle in a haystack" problem. An interesting CART subset analysis is described where the predictive capability of the technique for both productive hydrothermal and inferred EGS grid cells is encouraging. Conductive thermal modeling identified major variations in heat flow and T in the project area resulting from significant elevation differences between the basin and the range and) the geometry of a ~2-3km thick valley fill. This model was partly calibrated by pseudo-convection model which identified a large region of excess convection suggesting the presence of a hydrothermal system.

Baseline EGS favorability mapping based on the following three key parameters: T, rock type and stress, identified prospective EGS areas at the scale defined above. Trust mapping reflected the confidence in the data used for favorability mapping and identified areas for additional data development before exploratory drilling. Enhanced favorability/trust maps were not generated due to insufficient and/or verified information relative to the baseline dataset.

ACKNOWLEDGEMENTS

The project was conducted under the American Recovery and Reinvestment Act (ARRA) funding through the U.S. Department of Energy (DOE) and AltaRock Energy Inc., DOE contract no. DE-EE0002778. The author also extends a deep appreciation to other project technical team member, Trenton Cladouhos, Owen Callahan, Matthew Clyne, and Michael Swyer, all current or former members of AltaRock, Shane Smith, a PhD candidate at the University of Nevada Reno, Mahesh Thakur, a post doctorate researcher at Southern Methodist University during the study, and Virginia Maris, a post doctorate at the University of Utah Earth and Geoscience Institute. The authors thank Dr. David von Seggern at the University of Nevada Reno, for advice and support during the seismic portion of the project.

REFERENCES

AltaRock: EGS Exploration Methodology Project using the Dixie Valley Geothermal System, Nevada as a Calibration Site Part I—Final Scientific Report Baseline Conceptual Model, US Department of Energy DOE Award: DE-EE0002778, submitted to the National geothermal Data Repository, 2 January (2014a).

AltaRock: Exploration Methodology Project using the Dixie Valley Geothermal System, Nevada as a Calibration Site Part I—Final Scientific Report Enhanced Conceptual Model, US Department of Energy DOE Award: DE-EE0002778, submitted to the National geothermal Data Repository, 2 January (2014b).

Benoit, D.: Conceptual Models of the Dixie Valley, Nevada Geothermal Field, Geothermal Resources Council Transactions, v. 23, p. 505 - 511 (1999).

Benoit. D.: An Empirical Injection Limitation in Fault-Hosted Basin and Range Geothermal Systems, Geothermal Resources Council Transactions, v. 37, p. 888 - 894 (2013).

Biasi, G., Tibuleac, I., and Preston, L.: Regional resource area mapping in Nevada using the USArray Seismic Network. Geothermal Energy 2008 Conference and Expo, Reno, NV, Oct 5-8 (2008).

Blackwell, D. D., Bergman, S., Goff, F. Kennedy, B. M., McKenna, J. R., Richards, M. C., Smith, R. P., Waibel, A. F., and Wannamaker, P.: Description, Synthesis, and Interpretation of the Thermal Regime, Geology, Geochemistry and Geophysics of the Dixie Valley, Nevada Geothermal System, D. D. Blackwell and R. P. Smith, ed., unpublished DRAFT DOE Technical Report, 195p (2005).

Blackwell, D. D., Waibel, A. W., and Kelly, S. A.: Results of Dixie Valley Power Partners/Oxbow 1994 thermal gradient drilling program, unpublished report submitted to Oxbow Geothermal Corporation, Reno, Nevada (1994).

Blackwell, D. D., Steele, J. L. and Carter, L. S.: Heat-flow patterns of the North American continent: a discussion of the Geothermal Map of North America, in Slemmons, D. B., Engdahl, E. R., Zoback, M. D., and Blackwell, D. D., ed., Neotectonics of North America, Decade Map, v. 1, Geologic Society of America Bulletin, Boulder, CO, v. 103, p. 423–436 (1991).

Bogen N. L. and Cshwieckert, R. A: Magnitude of crustal extension across the Basin and Range Province: constraints from paleomagnetism, Earth and Planetary Science Letters, v. 75, p. 93-100 (1985).

Caskey, S. J., Wesnousky, S. G., Zhang, P., and Slemmons, D. B.: Surface Faulting of the 1954 Fairview Peak (Ms 7.2) and Dixie Valley (Ms 6.8) Earthquakes, Central Nevada. Bulletin of the Seismological Society of America, v. 86, no. 3, p. 761-787 (1996).

Hickman, S., Zoback, M., and Benoit, R.: Tectonic Controls on Reservoir Permeability in the Dixie Valley, Nevada Geothermal Field. Proceedings, 23rd Workshop on Geothermal Reservoir Engineering, Stanford University, California, Jan. 26-28, 8 p. (1998).

Hickman, S. H., Zoback, M. D., Barton, C. A., Benoit, R., Svitek, J., and Summers, R.: Stress and Permeability Heterogeneity within the Dixie Valley Geothermal Reservoir: Recent Results from Well 82-5. Proceedings, 25th Workshop on Geothermal Reservoir Engineering, Stanford University, California, Jan. 24-26, 10 p. (2000).

Iovenitti, J., Blackwell, D., Sainsbury, J., Tibuleac, I., Waibel, A., Cladouhos, T., Karlin, R., Kennedy, B. M., Isaaks, E., Wannamaker, P., Clyne, M., Callahan, O.: EGS Exploration Methodology Development using the Dixie Valley, Geothermal District as a Calibration Site: A Progress Report, Geothermal Resources Council Transactions, v. 35, p. 389 – 395 (2011).

Iovenitti, J., Blackwell, D., Sainsbury, J, Tibuleac, I., Waibel, A., Cladouhos, T., Karlin, R., Isaaks, E., Clyne, M., Ibser, F. H., Callahan, O., Kennedy, B. M., Wannamaker, P.: Towards Developing a Calibrated EGS Exploration Methodology Using the Dixie Valley Geothermal System, Nevada, Proceedings, 37th Eighth Workshop on Geothermal Reservoir Engineering Stanford University, Stanford, California, January 30- February 1 (2012).

Lachenbruch, A. H., and Sass, J. H.: Heat flow in the United States and the thermal regime of the crust. Heacock, J.G., editor, The Nature and Physical Properties of the Earth's Crust, American Geophysical Union Monograph, v. 20, p.626–675 (1997).

Palacky, G. J.: Resistivity characteristics of geologic targets: in, Electromagnetic methods in applied geophysics, M. N. Nabighian, ed., Soc. Explor. Geophys., Tulsa, OK, v. 1, 53-130 (1988).

Sasaki, Y.: Three-dimensional inversion of static-shifted magnetotelluric data: Earth, Planets and Space, 56, 239-248 (2004).

Smith, R.P., Wisian, K. W., Blackwell, D. D.: Geologic and Geophysical Evidence for Intra-basin and Footwall Faulting at Dixie Valley, Nevada. Geothermal Resources Council Transactions, v. 25, Aug. 26-69. 8 p, (2001).

Tibuleac, I., von Seggern, D., Iovenitti, J., Sainsbury, J., Biasi, G., Anderson, J.: EGS Exploration Methodology Development Using the Dixie Valley Geothermal District as a Calibration Site. The Seismic Analysis Component, Proceedings, 38th Eighth Workshop on Geothermal Reservoir Engineering Stanford University, Stanford, California, February 11-13 (2013).

Thakur, M., Blackwell, D. D., and Erkan, K.: The Regional Thermal Regime in Dixie Valley, Nevada, USA, Geothermal Resources Council Transactions, v. 36, p. 59 – 67 (2012).

MIT: The future of Geothermal Energy. Impact of Enhanced Geothermal Systems (EGS) on the United States in the 21st Century. Assessment by a Massachusetts Institute of Technology-led interdisciplinary panel (J.F. Tester, Chairman), 372pp (2006), http://geothermal.inel.gov/publications/future_of_geothermal_energy.pdf

Waibel, A. F.: An Overview of the Geology and Secondary Mineralogy of the High Temperature Geothermal Systems in Dixie Valley, Nevada. GRC Transactions, v. 11, p. 479-486, and GRC Bulletin, v. 16, no. 9, p. 5-13 (1987).

Wannamaker, P.E., Doerner, W.M., and Hasterok, D.P.: Cryptic Faulting and Multi-Scale Geothermal Fluid Connections in the Dixie Valley-Central Nevada Seismic Belt Area: Implications from MT Resistivity Surveying. Proceedings, 31st Workshop on Geothermal Reservoir Engineering, Stanford University, California, Jan. 30-Feb. 1, 8p (2006).

Wannamaker, P.E., Doerner, W.M., and Hasterok, D.P.: Integrated Dense Array and Transect MT Surveying at Dixie Valley Geothermal Area, Nevada; Structural Controls, Hydrothermal Alteration and Deep Fluid Sources. Proceedings, 32nd Workshop on Geothermal Reservoir Engineering, Stanford University, California, Jan. 22-24, 6p (2007).

Wannamaker, P., Maris, V., Sainsbury, J, and Iovenitti, J.: Intersecting Fault Trends and Crustal-Scale Fluid pathways Below the Dixie Valley Geothermal System, Nevada, Inferred from 3D Magnetotelluric Surveying, Proceedings, 38th Eighth Workshop on Geothermal Reservoir Engineering Stanford University, Stanford, California, February 11-13 (2013).

USGS: Assessment of Moderate- and High-Temperature Geothermal Resources of the United States, U.S. Department of the Interior, United States Geological Survey, fact Sheet 2008-3082, 4pp (2008).